J. Fluid Mech. (2004), *vol.* 516, *pp.* 303–334.
DOI: 10.1017/S002211200400062X Printed in the United Kingdom

Spherical capsules in three-dimensional unbounded Stokes flows: effect of the membrane constitutive law and onset of buckling

By E. LAC[1], D. BARTHÈS-BIESEL[1], N. A. PELEKASIS[2] AND J. TSAMOPOULOS[3]

[1]UMR CNRS 6600, Biomécanique et Génie Biomédical, Université de Technologie de Compiègne, France

[2]Department of Mechanical and Industrial Engineering, University of Thessaly, Greece

[3]Department of Chemical Engineering, University of Patras, Greece

(Received 28 February 2003 and in revised form 14 May 2004)

The dynamic response of an initially spherical capsule subject to different externally imposed flows is examined. The neo-Hookean and Skalak *et al.* (*Biophys. J.*, vol. 13 (1973), pp. 245–264) constitutive laws are used for the description of the membrane mechanics, assuming negligible bending resistance. The viscosity ratio between the interior and exterior fluids of the capsule is taken to be unity and creeping-flow conditions are assumed to prevail. The capillary number ε is the basic dimensionless number of the problem, which measures the relative importance of viscous and elastic forces. The boundary-element method is used with bi-cubic B-splines as basis functions in order to discretize the capsule surface by a structured mesh. This guarantees continuity of second derivatives with respect to the position of the Lagrangian particles used for tracking the location of the interface at each time step and improves the accuracy of the method. For simple shear flow and hyperbolic flow, an interval in ε is identified within which stable equilibrium shapes are obtained. For smaller values of ε, steady shapes are briefly captured, but they soon become unstable owing to the development of compressive tensions in the membrane near the equator that cause the capsule to buckle. The post-buckling state of the capsule is conjectured to exhibit small folds around the equator similar to those reported by Walter *et al. Colloid Polymer Sci.* Vol. 278 (2001), pp. 123–132 for polysiloxane microcapsules. For large values of ε, beyond the interval of stability, the membrane has two tips along the direction of elongation where the deformation is most severe, and no equilibrium shapes could be identified. For both regions outside the interval of stability, the membrane model is not appropriate and bending resistance is essential to obtain realistic capsule shapes. This pattern persists for the two constitutive laws that were used, with the Skalak *et al.* law producing a wider stability interval than the neo-Hookean law owing to its strain hardening nature.

1. Introduction

We consider the deformation of a liquid-filled capsule enclosed by a thin hyperelastic membrane, suspended in another flowing liquid. This situation is encountered in many biomedical or industrial applications where encapsulation of living cells, or of active agents in a protecting membrane, is necessary. It is then important to assess the

response of the capsule to the imposed external stresses and, in particular, to predict the onset of burst. However, experimental and theoretical studies have underlined the complex mechanical interaction of different physical properties of the capsule such as geometry, membrane constitutive law and rheology of the internal medium. Here, we concentrate on initially spherical capsules, filled with a Newtonian liquid with viscosity $\lambda\mu$ and study the influence of the membrane constitutive law on their motion and deformation when they are freely suspended in a three-dimensional Stokes flow with viscosity μ.

Some experimental results regarding the behaviour of artificial capsules in flow are available. In particular, Barthès-Biesel (1991) and Chang & Olbricht (1993*a*) have studied the deformation of artificial capsules freely suspended in a planar hyperbolic flow created in the centre of a four-roller flow cell. Chang & Olbricht studied the effect of shear rate on nylon membrane capsule deformation, but do not report any breakup of the particle in the range of tested shear rates. Barthès-Biesel reports that, under large shear stress, a capsule with a polylysine membrane develops high-curvature tips where the membrane is punctured.

Capsules in simple shear flow have been studied experimentally by Chang & Olbricht (1993*b*) and by Walter, Rehage & Leonhard (2000, 2001) in a counter-rotating Couette device. After a short transient time, the capsule reaches a steady shape around which the membrane rotates. This rotation, first described for red blood cells, is called the *tank-treading* motion (Schmid-Schönbein & Wells 1960). Consequently, the inner fluid of the capsule is still in motion and the value of the viscosity ratio λ affects the capsule response (Pfafferott, Wenby & Meiselman 1985). For $\lambda \ll 1$, Chang & Olbricht (1993*b*) find that the capsule will burst for large enough shear rates. The breakup point is located at the tip of the capsule, where the curvature is large. Walter *et al.* (2000) do not reach large enough shear rates to observe burst.

Asymptotic solutions for initially spherical capsules suspended in weak linear shear flows have been obtained by Barthès-Biesel (1980) and by Barthès-Biesel & Rallison (1981) who have calculated the deformation of the capsule. In simple shear flow, this model predicts the tank-treading motion of the membrane with an angular frequency equal to the suspending flow rotation rate. Large deformations of capsules in unbounded shear flow have been modelled numerically by a number of authors. Different membrane constitutive laws have been considered as well as different flow situations. In some cases, the membrane is assumed to be a thin sheet of a volume incompressible material described by a neo-Hookean elastic law (Li, Barthès-Biesel & Helmy 1988; Eggleton & Popel 1998; Ramanujan & Pozrikidis 1998; Diaz, Pelekasis & Barthès-Biesel 2000). Area incompressible membranes have been considered to model the behaviour of red blood cells (Eggleton & Popel 1998; Ramanujan & Pozrikidis 1998) or lipid vesicles (Kraus *et al.* 1996). The bending rigidity of the membrane has also been taken into account (Kraus *et al.* 1996; Kwak & Pozrikidis 2001; Pozrikidis 2001). On the numerical side, different versions of the boundary-integral method have been used for modelling large deformations of capsules in uniaxial extensional flow (Li *et al.* 1988; Pozrikidis 1990; Diaz *et al.* 2000; Kwak & Pozrikidis 2001) and in simple shear flow (Kraus *et al.* 1996; Navot 1998; Ramanujan & Pozrikidis 1998; Pozrikidis 2001). Eggleton & Popel (1998) used the immersed boundary method and were able to recover some findings of the above studies for the case of simple shear flow. However, owing to the additional computational load required by this method, they could only follow the capsule response over relatively short times.

The first study of the response of a spherical capsule suspended in simple shear flow (Pozrikidis 1995) predicted a critical value of the shear rate past which no equilibrium

could be obtained and burst was conjectured to occur. Ramanujan & Pozrikidis (1998) investigated the effect of the viscosity ratio λ and were able to follow the deformation of initially spherical, ellipsoidal or area-incompressible biconcave capsules over a wide range of shear rates. They concluded that the capsule showed no tendency to break up. Navot (1998) considered another constitutive law for the elastic tensions in the membrane, modelled as a network of connected springs. He was able to reach very large deformations and to investigate the long-time tank-treading motion of the membrane for $\lambda = 1$, and did not observe breakup of the capsule.

When an unstructured mesh is used to discretize the membrane (Navot 1998; Ramanujan & Pozrikidis 1998), it is necessary to resort to approximations to calculate the surface gradient of the elastic tensions in the membrane. In particular, the load is averaged over an element in the boundary integral. Although this procedure must converge towards the true solution as the mesh size decreases, it may induce smoothing out of a potential instability. Our own experience with axisymmetric problems involving large deformations of an elastic interface has shown the importance of a very precise description of the deformed membrane geometry. Diaz *et al.* (2000) used a cubic B-spline interpolation of the meridian of an axisymmetric capsule and obtained very good accuracy with a reasonable number of points. Hence, we have focused our efforts on a precise description of the three-dimensional membrane geometry and mechanics. Lagrangian tracking of the interface is performed and the mechanical problem is expressed in general curvilinear coordinates on a time-dependent Lagrangian mesh, as described in § 2.2. The boundary-element method is used in conjunction with surface interpolation by means of bi-cubic B-splines. This allows a continuous description of the geometric characteristics of the interface up to second-order properties, such as curvature. The first goal of this study is to show the efficiency of our numerical method in modelling large or small membrane deformation accurately. Then, we shall investigate the limit of validity of the mechanical model when bending resistance is neglected. We find that under small viscous load compared to elastic stresses, the equilibrium deformation of the capsule is unstable and that the membrane tends to buckle, as observed experimentally (Walter *et al.* 2001). The last goal is to study the influence on capsule deformation of different membrane constitutive laws and different Stokes flow situations. We shall consider only capsules with an initially spherical shape, which corresponds to the typical geometry of artificial capsules.

The physical problem (fluid dynamics and membrane mechanics) is presented briefly in § 2. Section 3 is devoted to the numerical method and its validation in terms of numerical convergence and comparison with previous numerical studies by Ramanujan & Pozrikidis (1998). Finally, results are presented for a spherical capsule in simple shear flow (§ 4), in hyperbolic flow (§ 5) and in axisymmetric elongational flow (§ 6). They are compared to theoretical predictions in the limit of small deformations, to previous numerical results and, when possible, to experimental data. An overall discussion is presented in the last section and directions for future work are proposed.

2. Problem statement

The physical assumptions related to the deformation and motion of deformable liquid-filled capsules are presented only briefly in this section, since it is now a classical problem. For further details, see papers by Barthès-Biesel *et al.* and by Pozrikidis *et al.*

2.1. *Motion of the internal and external liquids*

We consider an initially spherical capsule of radius a, consisting of a liquid droplet enclosed by an infinitely thin elastic membrane M, suspended in an unbounded shear

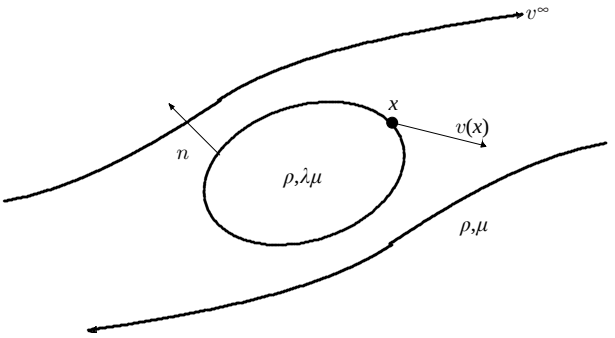

FIGURE 1. Capsule in Stokes flow.

flow of velocity $\boldsymbol{v}^\infty$ and shear rate $\dot{\gamma}$ (figure 1). Both fluids are supposed to be Newtonian and to have equal dynamic viscosity μ (i.e. $\lambda = 1$) and density ρ The interface obeys a simple membrane model, with negligible bending resistance. We also assume that it is purely elastic and characterized by a surface shear modulus G_s and an area dilation modulus K.

Computing the deformation and the position of the free surface requires the velocity field on the membrane. Because of the small dimensions of the particle, the Reynolds number $\rho\dot{\gamma}a^2/\mu$ is very small and the Stokes equations apply for both the internal and external fluid motion. Under this assumption, the interfacial velocity $\boldsymbol{v}$ at a point $\boldsymbol{x}$ on the membrane is expressed by means of an integral equation (Rallison & Acrivos 1978; Pozrikidis 1992)

$$\boldsymbol{v}(\boldsymbol{x}) = \boldsymbol{v}^\infty(\boldsymbol{x}) - \frac{1}{8\pi\mu} \oint_M \boldsymbol{J}(\boldsymbol{x}, \boldsymbol{y}) \cdot \Delta \boldsymbol{f}(\boldsymbol{y})\, \mathrm{d}S(\boldsymbol{y}), \tag{2.1}$$

where $\Delta \boldsymbol{f}$ represents the jump of viscous traction across the interface and the kernel $\boldsymbol{J}$ is a free-space Green's function defined as

$$J_{ij}(\boldsymbol{x}, \boldsymbol{y}) = \frac{\delta_{ij}}{r} + \frac{r_i r_j}{r^3}, \tag{2.2}$$

with $\boldsymbol{r} = \boldsymbol{x} - \boldsymbol{y}$ and $r = \|\boldsymbol{r}\|$.

2.2. *Membrane mechanics*

Since the membrane is supposed to be infinitely thin, the jump of viscous traction $\Delta \boldsymbol{f}$ is equal to the elastic load on the membrane. It is then related to the elastic tension tensor $\boldsymbol{T}$ in the interface by the membrane equilibrium equation

$$\nabla_s \cdot \boldsymbol{T} + \Delta \boldsymbol{f} = 0, \tag{2.3}$$

where ∇_s represents the gradient in the membrane surface. The problem is closed with a constitutive equation describing the elastic behaviour of the membrane.

The position of points at the interface is defined by means of two independent parameters θ^1 and θ^2. After the start of the flow, a material point $\boldsymbol{X}(\theta^1, \theta^2)$ of the unstressed membrane is convected to position $\boldsymbol{x}(\theta^1, \theta^2, t)$. Consequently, the kinematic condition at the interface reads

$$\frac{\partial}{\partial t}\boldsymbol{x}(\theta^1, \theta^2, t) = \boldsymbol{v}(\boldsymbol{x}, t). \tag{2.4}$$

The membrane mechanics problem is expressed in the curvilinear coordinate system defined by θ^1 and θ^2 (Green & Adkins 1960). Note that the convected coordinate lines

$\theta^\alpha =$ constant do not necessarily coincide with the principal directions of deformation. Except when indicated, Greek indices are equal to 1 or 2, and repeated indices are summed. Capital and lowercase letters denote quantities in the initial unstressed and deformed states, respectively. Local covariant and contravariant basis $(\boldsymbol{a}_1, \boldsymbol{a}_2, \boldsymbol{n})$, $(\boldsymbol{a}^1, \boldsymbol{a}^2, \boldsymbol{n})$, $(\boldsymbol{A}_1, \boldsymbol{A}_2, \boldsymbol{N})$ and $(\boldsymbol{A}^1, \boldsymbol{A}^2, \boldsymbol{N})$ are defined where $\boldsymbol{n}$ and $\boldsymbol{N}$ denote unit outer normal vectors to the surface and where the non-unit tangent vectors to coordinate lines are $\boldsymbol{a}_\alpha = \partial \boldsymbol{x}/\partial\theta^\alpha$ and $\boldsymbol{A}_\alpha = \partial \boldsymbol{X}/\partial\theta^\alpha$. The components of the associated metric tensors are $a_{\alpha\beta} = \boldsymbol{a}_\alpha \cdot \boldsymbol{a}_\beta$, $\boldsymbol{A}_{\alpha\beta} = \boldsymbol{A}_\alpha \cdot \boldsymbol{A}_\beta$, etc. Invariants of the transformation may be defined as (Green & Adkins 1960)

$$I_1 = A^{\alpha\beta}a_{\alpha\beta} - 2 = \lambda_1^2 + \lambda_2^2 - 2, \quad I_2 = \det(A^{\alpha\beta})\det(a_{\alpha\beta}) - 1 = J_s^2 - 1, \tag{2.5}$$

where λ_1 and λ_2 denote the extension ratios in the principal strain directions. Physically, $J_s = \lambda_1\lambda_2$ represents the ratio between the deformed and the undeformed local surface areas.

In the case of a plane isotropic hyperelastic material, the contravariant components of the tension tensor $\boldsymbol{T}$ are related to a strain energy function $W(I_1, I_2)$,

$$T^{\alpha\beta} = \frac{2}{J_s}\frac{\partial W}{\partial I_1}A^{\alpha\beta} + 2J_s\frac{\partial W}{\partial I_2}a^{\alpha\beta}. \tag{2.6}$$

The membrane equilibrium equation (2.3) becomes

$$\frac{\partial T^{\alpha\beta}}{\partial\theta^\alpha} + \Gamma^\alpha_{\alpha\lambda}T^{\lambda\beta} + \Gamma^\beta_{\alpha\lambda}T^{\alpha\lambda} + \Delta f^\beta = 0 \quad (\beta = 1, 2), \tag{2.7}$$

$$T^{\alpha\beta}b_{\alpha\beta} + \Delta f^n = 0,$$

where the load is expressed in the local covariant basis $\Delta\boldsymbol{f} = \Delta f^\beta \boldsymbol{a}_\beta + \Delta f^n \boldsymbol{n}$. The Christoffel symbols are defined by $\Gamma^\beta_{\alpha\lambda} = (\partial\boldsymbol{a}_\alpha/\partial\theta^\lambda)\cdot\boldsymbol{a}^\beta$ and the curvature tensor by $b_{\alpha\beta} = \boldsymbol{n}\cdot(\partial\boldsymbol{a}_\alpha/\partial\theta^\beta)$.

2.3. *Constitutive equation for the elastic tensions*

Barthès-Biesel, Diaz & Dhenin (2002) discussed different constitutive laws classically used to describe thin hyperelastic interfaces. Membranes made of polymerized media are usually modelled as thin sheets of a volume-incompressible isotropic material with initial uniform thickness. The area dilation due to deformation is then balanced by the thinning of the membrane. The simplest constitutive equation is then the two-dimensional form of the neo-Hookean law (NH)

$$W^{NH} = \tfrac{1}{2}G_s\left(I_1 - 1 + \frac{1}{I_2 + 1}\right). \tag{2.8}$$

where G_s is the surface shear elastic modulus. Ramanujan & Pozrikidis (1998) used another version of (2.8), which they call the *zero-thickness shell* formulation

$$W^{RP} = \tfrac{1}{2}G_s\left[I_1 - \log(I_2 + 1) + \tfrac{1}{2}\log^2(I_2 + 1)\right]. \tag{2.9}$$

The two strain energy functions W^{NH} and W^{RP} are equivalent for small deformation, but lead to different tension–deformation relations for large strains.

Starting from general principles of elasticity, Skalak *et al.* (1973) proposed another law (SK), valid for plane-isotropic materials

$$W^{SK} = \tfrac{1}{4}G_s\left(\left(I_1^2 + 2I_1 - 2I_2\right) + C\left(J_s^2 - 1\right)^2\right). \tag{2.10}$$

The first term of the right-hand side of (2.10) accounts for shearing effects, while the second term accounts for area dilation, with associated moduli G_s and CG_s. The

SK law, initially proposed for area incompressible biological membranes ($C \gg 1$), can also be used to model other interfaces for which C is of order 1.

The neo-Hookean law and the Skalak *et al.* law are linear in the domain of small deformations, with surface Poisson ratio given, respectively, by $\nu_s = 1/2$ and $\nu_s = C/(1+C)$, surface Young modulus by $E_s^{NH} = 3G_s$ and $E_s^{SK} = 2G_s(2+C)/(1+C)$, area dilation modulus by $K^{NH} = 3G_s$ and $K^{SK} = G_s(1+2C)$. For $C = 1$, the NH and SK laws have the same small-deformation behaviour. For large strains, however, they predict different material responses. For example, in uniaxial extension, the NH law appears to be strain-softening, whereas the SK law is strain hardening (Barthès-Biesel *et al.* 2002).

Navot (1998) has introduced a constitutive law for a polymeric material described as a network of connected springs. In the continuum limit, it is equivalent to the strain energy

$$W = kI_1, \tag{2.11}$$

where k is an elastic constant of the material. This law allows for very large deformations of the capsule, as discussed in § 4.2.

Dimensional analysis of the problem shows that an important parameter is the capillary number $\varepsilon = \mu\dot{\gamma}a/G_s$, which measures the ratio between the viscous forces exerted by the fluids and the elastic resistance of the membrane. Note that $\varepsilon = 3G$, where $G = \mu\dot{\gamma}a/E_s$ is the capillary number based on Young's modulus, used by Ramanujan & Pozrikidis (1998). In addition, $\varepsilon = 3p/10$ where p is the dimensionless shear rate used by Navot (1998).

It is usually possible to obtain an equilibrium solution to the set of equations (2.3)–(2.11), but the stability of this solution must be checked. Indeed, if compression occurs, it is well known from shell theory (Timoshenko & Gere 1961) that a thin shell will buckle when the compressive stress exceeds a critical value. For small deformations, this value is proportional to the bending modulus of the shell. Buckling leads to deformations normal to the shell plane with a wavelength that is also proportional to the bending modulus. Consequently, if the capsule interface has no bending stiffness, as assumed here through (2.3), it cannot sustain any compressive stress and will buckle as soon as one of the two principal tensions becomes negative. A simple stability criterion is thus that the tensions T_1 and T_2 in the principal strain directions 1 and 2 should both be positive. When parameter C vanishes in the SK law, we note that the condition $T_\alpha \geqslant 0$ is equivalent to $\lambda_\alpha \geqslant 1$ ($\alpha = 1, 2$). This means that the membrane must be stretched in the two principal directions simultaneously. In our case, we did not find a deformed shape for which the volume is conserved and the membrane is stretched everywhere in both directions. Consequently, we considered values of C greater than zero, for which the area dilation modulus is always larger than the shear modulus.

For the strain energy function (2.11), we find from (2.6) that $T_1 = k\lambda_1/\lambda_2$ and $T_2 = k\lambda_2/\lambda_1$. The tensions are always positive and the membrane is stretched everywhere whatever its deformation may be.

3. Numerical method

3.1. *Boundary-element method*

In order to evaluate the forces on the membrane, to determine the metrics of the surface and, finally, to obtain the interfacial velocity by numerical integration, we must interpolate the position vector as well as the other dependent variables of the

problem on the surface of the capsule. A classical approach to interface tracking for deformable particles uses a structured mesh (e.g. Li *et al.* 1988; Pozrikidis 1990, 1995) that is defined through a proper parametric description of the interface. In the latter study, for example, the surface nodes are defined by means of the meridional and azimuthal angles, whereas a flat triangular representation is adopted for the surface elements. However, questions were raised by Ramanujan & Pozrikidis (1998) as to the reliability of this approach, owing to the singular nature of the two poles. This has led to an increasing interest in unstructured mesh descriptions, because of the larger flexibility that they offer, despite increased complexity in local topology. Indeed, several investigators have discretized the surface with an unstructured grid using flat triangular elements (e.g. Kraus *et al.* 1996; Navot 1998) or with bi-quadratic six-node triangular elements (e.g. Ramanujan & Pozrikidis 1998). In this context, Ramanujan & Pozrikidis (1998) and Navot (1998) concluded that a steady shape existed for initially spherical capsules under external simple shear flow, irrespective of the shear rate intensity. This reverts the findings of Pozrikidis (1995) with a structured mesh, namely that a critical shear rate exists beyond which the capsule continuously elongates and finally bursts. In an effort to resolve this issue and in view of the very good performance of boundary elements on cubic B-splines in axisymmetric configurations (Diaz *et al.* 2000), we decided to extend this method to model general surfaces. To this end, we use a structured mesh and describe the surface of the capsule with bi-cubic B-spline functions that depend on two independent parameters θ^1 and θ^2. After the start of the flow, the position $\boldsymbol{x}$ of a point on the membrane at time t is expressed as a sum of cubic polynomial basis functions B_k

$$\boldsymbol{x}(\theta^1, \theta^2, t) = \sum_{k,l} \bar{\boldsymbol{x}}_{kl}(t) B_k(\theta^1) B_l(\theta^2), \tag{3.1}$$

where $\bar{\boldsymbol{x}}_{kl}$ are the spline coefficients associated with $\boldsymbol{x}$. In this fashion, it is convenient to interpolate any dependent variable as a function of θ^α, while the degree and nature of the basis functions ensures continuity of $\boldsymbol{x}$ and of its derivatives up to second order along the interface (Prenter 1989). Consequently, the covariant basis vector $\boldsymbol{a}_1$ can then be calculated as

$$\boldsymbol{a}_1 = \frac{\partial \boldsymbol{x}}{\partial \theta^1} = \sum_{k,l} \bar{\boldsymbol{x}}_{kl}(t) B_k'(\theta^1) B_l(\theta^2), \tag{3.2}$$

where primed variables denote differentiation of single variable functions. The second derivatives of the position vector are similarly calculated in order to evaluate the Christoffel symbols, the curvature tensor and the surface gradient of the elastic tensions that appear in (2.7). This method allows for direct calculation of $\Delta \boldsymbol{f}$, that is continuous along the interface. In the method proposed by Pozrikidis (1995) for an unstructured mesh, the single-layer integral is approximated in each element through the product between the average traction discontinuity and the free space kernel.

At time $t = 0$, θ^1 and θ^2 correspond to the azimuthal and meridional angles θ and ϕ in spherical coordinates. The initially spherical shape is discretized with $n \times m$ elements, corresponding to equal intervals of θ^1 and θ^2. For the description of any scalar variable, a total of $(n+3) \times (m+3)$ unknown spline coefficients are required (Prenter 1989). For example, for each component of the interfacial velocity $\boldsymbol{v}$, the discrete form of (2.1) provides one equation per node. Additional conditions follow from periodicity properties. In the present study, the surface of the sphere

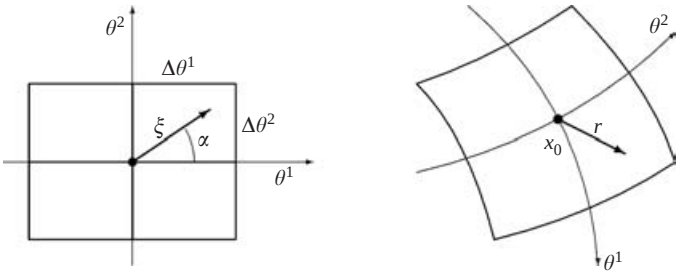

FIGURE 2. Polar co-ordinates (ξ, α) in the parametric domain (θ^1, θ^2) used to calculate the $1/r$ singular integral over the four neighbouring elements of the node $\boldsymbol{x}_0$.

was discretized with a minimum of 10×20 elements and a maximum of 50×100 elements.

The integral in (2.1) is calculated by means of regular Gaussian quadrature in each element where kernel $\boldsymbol{J}$ is not singular. However, each node belongs to four neighbouring elements in which the Euclidian distance r may vanish and where the single-layer kernel $\boldsymbol{J}$ may become singular (see (2.2)). Even if the Gauss points, where the integrand is calculated, never coincide with the nodes themselves, the distance r becomes small enough to generate large errors in the integral. To prevent this drop of accuracy, we calculate the integral in all the neighbouring elements using polar coordinates (ξ, α) defined in the parametric domain (θ^1, θ^2), with the singular point as the origin as shown in figure 2. This transformation introduces a Jacobian that approaches zero as fast as r, thus eliminating the effect of the singularity in the single-layer kernel.

Once the velocity is calculated, the nodes on the surface are convected through numerical integration of (2.4) with a fourth-order accurate Runge–Kutta method. Since the time integration is explicit, the stability of the numerical scheme restricts the value of the time step Δt. The latter must be decreased as mesh refinement increases and as ε decreases (Diaz *et al.* 2000). Typical dimensionless time steps $\dot{\gamma}\Delta t$ were taken in the range 10^{-4} to 10^{-2}. Once numerical stability is established, reducing the time step has no significant influence on the solution, indicating that the dominant error is due to spatial discretization.

3.2. *Validation of the numerical method*

A set of numerical simulations is presented as a validation of the convergence and accuracy of our numerical scheme. A comparison with previous numerical studies is also presented. We focus on the case of an initially spherical capsule with a neo-Hookean membrane placed in simple shear flow, an inherently three-dimensional flow situation that was already studied in detail by Ramanujan & Pozrikidis (1998). The undisturbed velocity field $\boldsymbol{v}^\infty$ is given by

$$v_1^\infty(\boldsymbol{x}) = \dot{\gamma} x_2; \quad v_2^\infty(\boldsymbol{x}) = v_3^\infty(\boldsymbol{x}) = 0. \tag{3.3}$$

Immersed in this flow field, the capsule elongates along a direction at an angle Φ with respect to the flow direction, as a result of the torque exerted on it in the plane of shear. After a transient stage, the membrane particles acquire a steady trajectory, where the normal component of the interfacial velocity vanishes while the tangential component remains finite. Consequently, the membrane material points exhibit a continuous rotational motion along the steady deformed surface. This periodic tank-treading motion has been captured numerically by Ramanujan & Pozrikidis (1998)

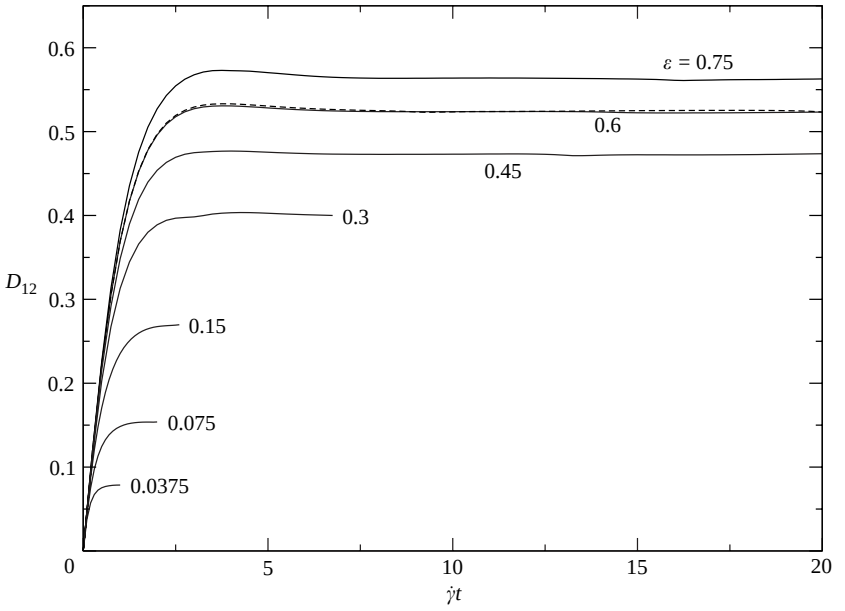

FIGURE 3. Time evolution of the deformation D_{12} for different values of ε for a capsule with an NH membrane in simple shear flow. For $\varepsilon = 0.6$, the two curves show the influence of the initial position of the poles: on the x_2-axis (solid line) and on the x_1-axis (dashed line).

and by Navot (1998) as a function of capillary number. For moderate shear rates, the deformed shape is close to an ellipsoid. The three-dimensional deformation can be then measured by the Taylor parameter D_{ij}

$$D_{ij} = \frac{|L_i - L_j|}{L_i + L_j} \quad (i, j = 1, 2, 3), \tag{3.4}$$

where L_1, L_2 and L_3 denote the three semi axis lengths of the ellipsoid that has the same inertia tensor as the capsule. For any value of ε we follow the variation with time of the deformation D_{12} in the shear plane as a function of time $\dot{\gamma}t$, until an equilibrium value D_{12}^{∞} is reached (figure 3).

The case $\varepsilon = 0.6$, for which the capsule reaches a significant deformation of the order of 50% is studied in detail. Computations were performed with different time steps and different spatial grids. For a 20×40 mesh and dimensionless time steps $\dot{\gamma}\Delta t$ decreased from 0.01 to 0.001, the equilibrium deformation values differed by less than 10^{-5}. Similarly, for $\dot{\gamma}\Delta t = 0.005$, when the mesh was refined from 20×40 to 30×60 elements, the relative variation of D_{12}^{∞} was lower than 1.2% between the coarser and finer grids. When the mesh was further refined from 30×60 to 40×80 elements, the difference in values of D_{12}^{∞} was less than 0.4%. An alternative measurement of the accuracy of the numerical scheme is obtained by monitoring the relative volume change of the capsule $\Delta V/V_0$, which should, of course, vanish since the capsule is volume incompressible. For 30×60 and 40×80 elements, the relative volume variation was of the order of 10^{-5} or less, even after long simulations (10^3 to 10^4 time steps). We thus conclude that the numerical method converges in time and space.

The structured mesh introduces a heterogeneity in the element size over the capsule interface. The influence of the initial position of the poles was studied by placing the

two poles in the plane of shear either on the x_1- or on the x_2-axis. As shown on figure 3, there is no significant difference between the values of the steady deformation. However, when the poles were placed on the x_3-axis, an instability sets in. This effect is also reported by Pozrikidis (1995).

Finally, we compared our results obtained with membrane constitutive law (2.8) to those of Ramanujan & Pozrikidis (1998) for membrane constitutive law (2.9). Our value of D_{12}^{∞} exceeds by 4% that of Ramanujan & Pozrikidis, because the strain energy functions of the membrane are different in the large-deformation domain. However, when we used our method to compute the deformation of a capsule that obeys law (2.9), our values for D_{12}^{∞} are higher by about 1.3% than those of Ramanujan & Pozrikidis. This may be attributed to the difference in numerical procedures. As was also indicated by Ramanujan & Pozrikidis (1998), we note that the deformation of the neo-Hookean membrane is slightly larger than that obtained with the zero-thickness shell law.

4. Capsules in simple shear flow

We now investigate the dynamic behaviour of an initially spherical capsule in response to an external simple shear flow with increasing magnitude of the imposed shear rate. The poles are initially located on the x_2-axis. The capsule first elongates and then reaches an equilibrium state where the membrane material points rotate continuously around the steady deformed shape. As an example, figure 3 shows the time evolution of D_{12} for a range of values of ε and a neo-Hookean membrane. The value of the equilibrium deformation parameter D_{12}^{∞} corresponds to the plateau of the curves.

Some new results are also presented for a capsule with a membrane that obeys the SK law, with three finite values of the area dilation modulus, corresponding to finite values of C in the range [0.5, 10]. Values of C larger than 10 were not investigated because the stability of the numerical scheme requires smaller time steps as C increased, thus leading to prohibitively long computing times. However, $C = 10$ corresponds to a membrane with an area dilation modulus 21 times larger than the shear modulus. The dynamics of such a membrane are then dominated by near-area incompressibility and reach an asymptotic state independent of the exact value of C (Barthès-Biesel *et al.* 2002). Figure 4(*a*) shows the dependence of D_{12}^{∞} on ε for capsules with an NH or an SK membrane, as well as the results of Ramanujan & Pozrikidis (1998). According to the latter authors, the capsule always reaches a steady deformed shape, irrespective of the shear rate level. We find instead that a stable equilibrium state is obtained only within an interval $[\varepsilon_L, \varepsilon_H]$ of values of ε that depend on the membrane constitutive law. The different behaviours that are observed are discussed in detail in the following subsections.

4.1. *Low shear rates* ($\varepsilon < \varepsilon_L$)

The equilibrium deformation D_{12}^{∞} of a capsule is plotted as a function of the dimensionless shear rate ε in figure 4(*b*) (insert) for small deformations. In this limit, Barthès-Biesel & Rallison (1981) calculated an asymptotic expression of the steady deformation, which was generalized later by Barthès-Biesel *et al.* (2002) to any value of ν_s

$$D_{12}^{\infty} = \frac{5}{4}\frac{2+\nu_s}{1+\nu_s}\varepsilon. \tag{4.1}$$

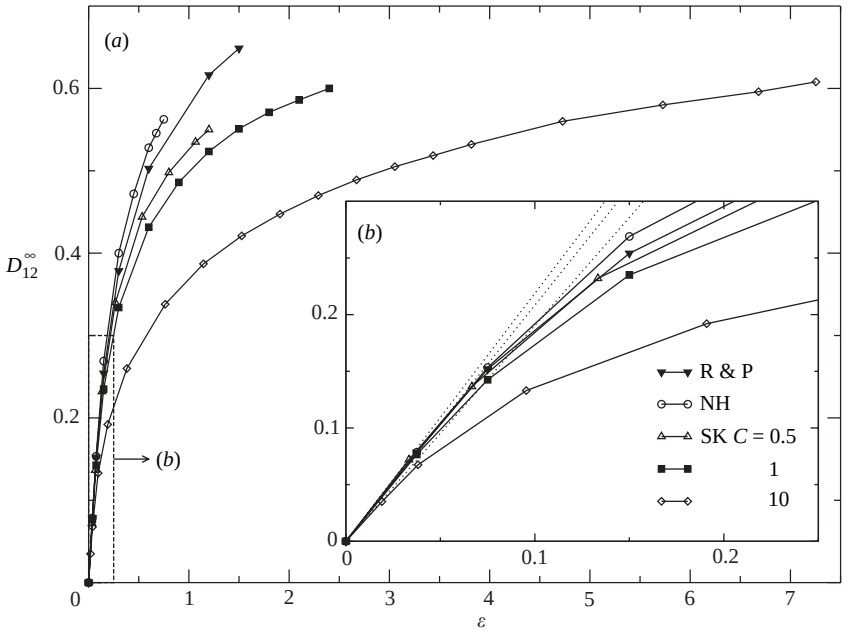

FIGURE 4. Steady deformation D_{12}^{∞} as a function of capillary number ε for different membrane laws; 'R&P' corresponds to results by Ramanujan & Pozrikidis (1998). Insert (b): zoom view for small ε where dotted lines represent asymptotic predictions by Barthès-Biesel *et al.* (2002) for $\nu_s = 1/3$ (SK $C = 0.5$), $\nu_s = 1/2$ (NH, SK $C = 1$) and $\nu_s = 10/11$ (SK $C = 10$); increasing ν_s correspond to decreasing slopes.

This result is recovered within 2% up to $\varepsilon = 0.075$, approximately for a capsule with a NH membrane. For a capsule with a SK membrane and $C = 1$, the small ε results are asymptotically identical to those obtained with the NH law (figure 4*b*). For $C = 0.5$ and 10, the numerical results also follow the predictions of the small deformation theory (corresponding to $\nu_s = 0.33$ and 0.909, respectively). For $C = 10$, the agreement between the numerical and asymptotic values of D_{12}^{∞} is restricted to a much narrower range of ε values, compared to the cases with $C = 0.5$ and 1 or with an NH membrane.

However, even when the deformation is small, the tank-treading motion of the membrane could not be captured for a full circumvolution because of an instability which is due to compression zones on the membrane, where at least one of the two principal elastic tensions becomes negative. To illustrate the point, we study a capsule with an NH membrane at a time when the equilibrium deformation plateau is reached. The principal elastic tension distribution in the shear plane x_1, x_2 is represented as a function of θ^1 in figures 5(a) and 5(b) for a range of values of ε corresponding to moderate deformations of the membrane. On this graph, direction 1 lies in the shear plane and direction 2 is orthogonal to this plane. Tension T_2 takes negative values in the vicinity of the capsule equator where the membrane is compressed and tends to buckle (see § 2.4).

Barthès-Biesel (1980) studied the deformation of an initially spherical capsule suspended in a simple shear flow in the limit of small ε. To first order in ε, the load on the membrane is given by

$$\Delta \boldsymbol{f} = 5\mu \boldsymbol{e} \cdot \frac{\boldsymbol{x}}{a}, \tag{4.2}$$

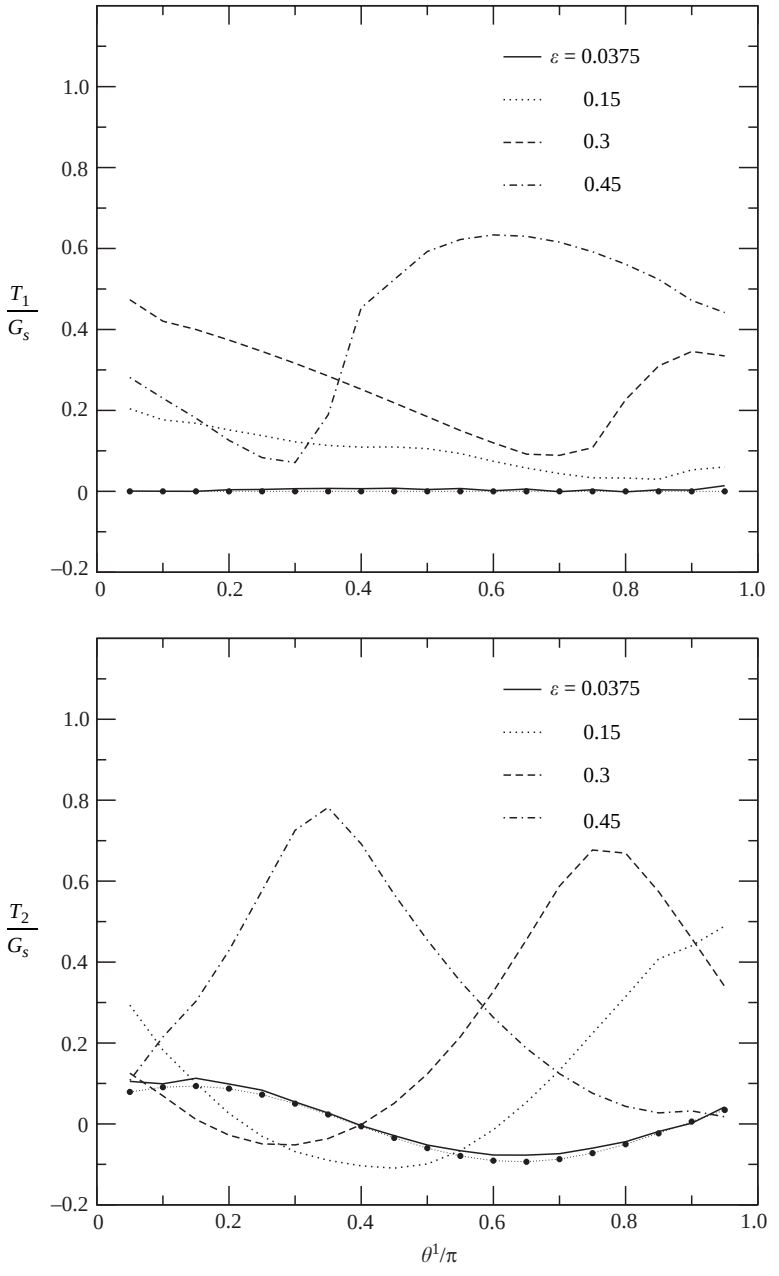

FIGURE 5. Principal tensions T_1 and T_2 in the shear plane (x_1, x_2) for different values of ε (NH membrane); ●, the analytical solution for $\varepsilon = 0.0375$.

where $\boldsymbol{e}$ is the rate of strain tensor of the undisturbed flow field. The equilibrium equation (2.7) can be solved for a sphere and the components of the elastic tensions (expressed in a unit vector basis) are given by

$$\frac{T^{\theta\theta}}{G_s} = \frac{5\varepsilon}{2}\sin 2\phi, \quad \frac{T^{\phi\theta}}{G_s} = \frac{5\varepsilon}{2}\cos\theta\cos 2\phi, \quad \frac{T^{\phi\phi}}{G_s} = -\frac{5\varepsilon}{2}\cos^2\theta\sin 2\phi, \tag{4.3}$$

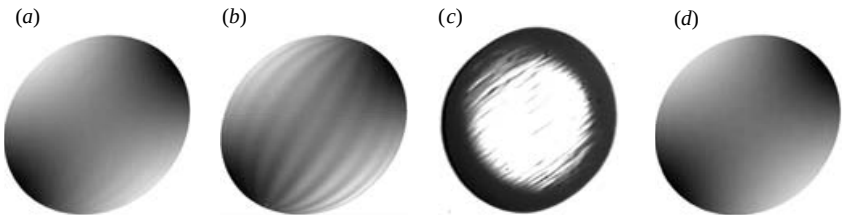

FIGURE 6. Three-dimensional representation of a capsule in simple shear flow ($\varepsilon = 0.0375$, NH membrane); grey-level map represents the normal load q^n (*a*) at $\dot{\gamma}t = 0.9$ and (*b*) at $\dot{\gamma}t = 1$. (*c*) Buckling of an initially spherical capsule with an organosiloxane membrane in simple shear flow (Walter *et al.* 2001). (*d*) Pre-inflated capsule at $\dot{\gamma}t = 2$.

where $(r, \theta, \phi$ define spherical coordinates such that the positive x_3 semi axis corresponds to $\theta = 0$ and the x_1x_3 plane corresponds to $\phi = 0$. For membrane points in the shear plane ($\theta = \pi/2$), the principal tension values are

$$\frac{T_\theta}{G_s} = \frac{5\varepsilon}{2}\sin 2\phi, \quad \frac{T_\phi}{G_s} = 0. \tag{4.4}$$

Thus, the asymptotic theory predicts that part of the membrane, corresponding to $\phi \in [\pi/2, \pi] \cup [3\pi/2, 2\pi]$ is under compression. With the numerical model notations, T_1 and T_2 are equivalent to T_φ and T_θ in the shear plane, respectively. For $\varepsilon = 0.0375$, there is very good agreement between the asymptotic and numerical values of tension. Indeed, T_1 is very small and T_2 follows closely the sinusoidal law (4.4), as shown on figure 5(*b*). When ε increases, the asymptotic theory is no longer valid, but tension T_2 still takes negative values on part of the membrane located near the middle of the elongated capsule. This occurs up to a limiting value of ε, roughly $\varepsilon_L = 0.45$. Since there is no bending stiffness, the compressed membrane points tend to draw nearer and eventually to overlap, and consequently the numerical model breaks down. Numerically, the onset of buckling is detected by the appearance of oscillations in the membrane point position that lead to the formation of folds. This behaviour is illustrated on three-dimensional representations of the capsule obtained for $\varepsilon = 0.0375$ at times corresponding to the initial stage of the equilibrium plateau (figure 6*a*) and shortly after (figure 6*b*). In figure 6(*a*, *b*), the grey-level mapping corresponds to the normal load value which tends to oscillate near the capsule equator, thus leading to local oscillation of one principal curvature sign. The compression of the membrane occurs near the equator of the deformed capsule as predicted by the asymptotic theory for vanishingly small values of ε. It should be pointed out that since there is no bending resistance to determine a specific buckling wavelength, the folds that are detected depend on the grid-point spacing and do not correspond to the actual buckling phenomenon. However, folds do occur and have been observed experimentally by Walter *et al.* (2001) who studied the deformation of spherical artificial capsules suspended in simple shear flow. The capsule shown on figure 6(*c*) has an initial radius of 343 μm and a membrane made of polysiloxane with a nearly zero Poisson ratio, and thus with nearly equal values of shear and area dilation modulus. The folds are indeed located also about the equator and have the same orientation as those shown in figure 6(*b*).

We conclude that the instability is not of numerical origin, but is due to the simplification used in the mechanical model of the interface when bending stiffness is neglected. These negative elastic tensions were predicted long ago by the asymptotic theory of Barthès-Biesel (1980) and have also been reported in the numerical findings

	NH $\nu_s = 0.5;\ K/G_s = 3$	SK ($C = 0.5$) $\nu_s = 0.333;\ K/G_s = 2$	SK ($C = 1$) $\nu_s = 0.5;\ K/G_s = 3$	SK ($C = 10$) $\nu_s = 0.909;\ K/G_s = 21$
(a)	$\varepsilon_L = 0.45$ $(D_{12}^{\infty})_L = 0.47$	$\varepsilon_L = 0.8$ $(D_{12}^{\infty})_L = 0.5$	$\varepsilon_L = 0.4$ $(D_{12}^{\infty})_L = 0.37$	$\varepsilon_L = 0.06$ $(D_{12}^{\infty})_L = 0.09$
	$\varepsilon_H = 0.63$ $(D_{12}^{\infty})_H = 0.53$	$\varepsilon_H \approx 1.2$ $(D_{12}^{\infty})_H \approx 0.55$	$\varepsilon_H = 2.4$ $(D_{12}^{\infty})_H = 0.6$	$\varepsilon_H \approx 7.5$ $(D_{12}^{\infty})_H \approx 0.61$
(b)	$\varepsilon_L = 0.14$ $(D_{12}^{\infty})_L = 0.46$	$\varepsilon_L = 0.21$ $(D_{12}^{\infty})_L = 0.47$	$\varepsilon_L = 0.15$ $(D_{12}^{\infty})_L = 0.36$	$\varepsilon_L = 0.03$ $(D_{12}^{\infty})_L = 0.09$
	$0.21 < \varepsilon_H < 0.24$ $(D_{12}^{\infty})_H \approx 0.57$	$0.4 < \varepsilon_H < 0.53$ $(D_{12}^{\infty})_H \approx 0.57$	$0.6 < \varepsilon_H < 0.75$ $(D_{12}^{\infty})_H \approx 0.6$	$1.35 < \varepsilon_H < 1.53$ $(D_{12}^{\infty})_H \approx 0.56$

TABLE 1. Approximate stability domain for different membrane laws and flows. (a) Simple shear flow, (b) planar hyperbolic flow. For $\varepsilon < \varepsilon_L$, the membrane buckles; for $\varepsilon > \varepsilon_H$, no steady solution is obtained.

of Pozrikidis (1995). However, their significance regarding the stability of the solution had not been appreciated until now. It should be noted also that the steady deformation obtained for small ε values by previous authors (Pozrikidis 1995; Ramanujan & Pozrikidis 1998; Eggleton & Popel 1998) is always reported for small times, that is, when equilibrium is first reached (as in figure 6a), but when oscillations have not yet set in. Finally, a membrane that obeys Navot's law is always undergoing extension, as pointed out in § 2.3, and thus never shows any tendency towards buckling.

To stress this point, we have also studied the deformation of a pre-inflated capsule in the range of small ε. Starting with a spherical capsule with unstressed radius a_0, we apply an internal pressure (equivalent to an osmotic pressure) that creates an isotropic tension $T^p = 2K\Delta a/a_0$ and increases the capsule radius by Δa ($\Delta a \ll a_0$). The pre-stressed capsule is then subjected to simple shear flow with $\varepsilon = 0.0375$, where ε is based the new radius $a_0 + \Delta a$. For $\Delta a/a_0 = 0.015$, the pre-stress T^p is just superior to the minimum principal tension. The membrane is thus no longer under compression and the capsule reaches an equilibrium deformed shape (figure 6d) without any folds. The pre-stressed capsule stable deformation ($D_{12}^{\infty} = 0.068$) is slightly smaller than the unstable steady deformation ($D_{12}^{\infty} = 0.078$) obtained for the unstressed capsule for the same ε.

Accounting for a finite bending stiffness of the membrane (e.g. Pozrikidis 2001) would probably also allow us to continue the computation until a steady deformed shape is obtained (with or without folds, depending on the bending modulus). This is, however, outside the scope of this study, but will be discussed briefly in § 7.

A capsule with a membrane that obeys the SK law exhibits the same tendency towards buckling at low shear rates. The compressed zones are also located near the equator. However, the limiting value ε_L and the corresponding equilibrium deformation decrease as C increases, as shown in table 1. This may be attributed to the strain-hardening behaviour of the SK membrane, for which higher tensions develop for lower deformation as C increases.

4.2. *High shear rates* ($\varepsilon > \varepsilon_H$)

When the capillary number exceeds a value ε_H, the capsule does not reach a steady deformation. According to our computations, $\varepsilon_H = 0.75$ is approximately the upper bound for stable steady deformation of a capsule with a neo-Hookean membrane in

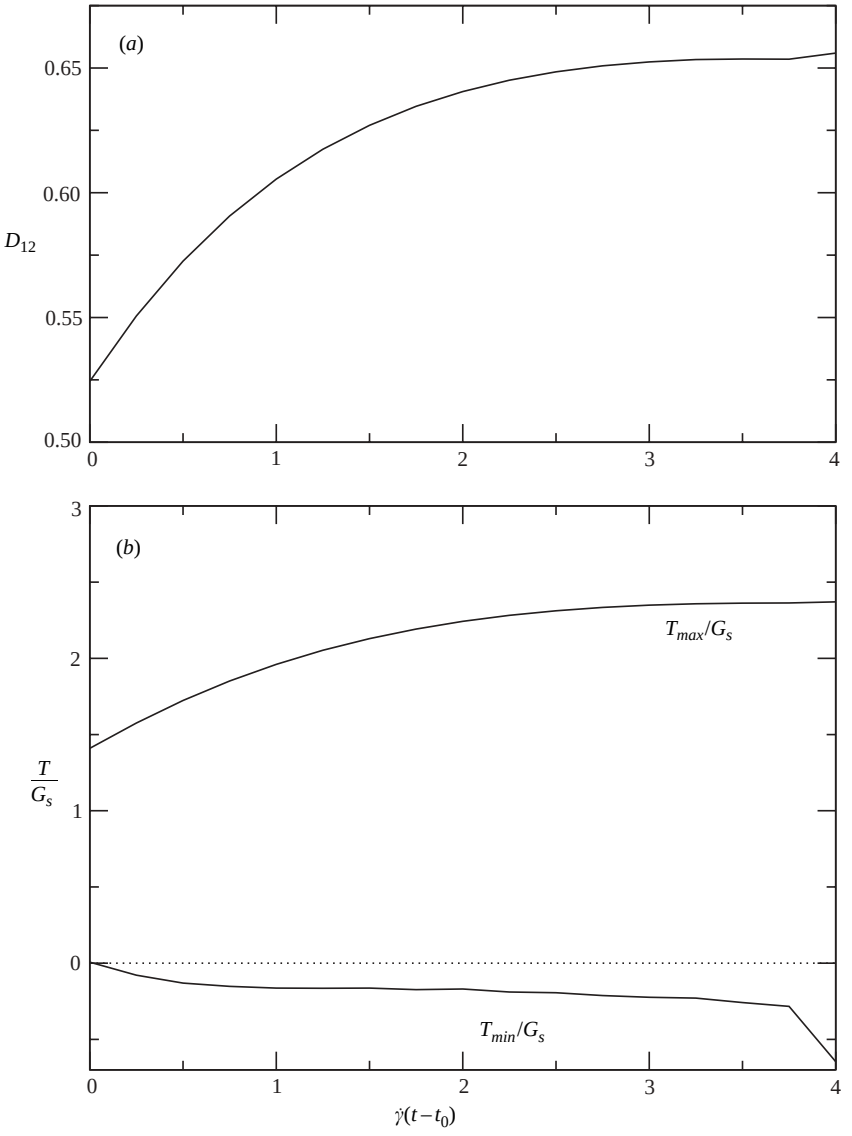

FIGURE 7. (*a*) Deformation and (*b*) minimum and maximum principal tension in the membrane for a capsule in simple shear flow (NH law, $\varepsilon = 1.2 > \varepsilon_H$). The simulation was restarted from the stable steady deformed shape obtained for $\varepsilon = 0.6$ at $\dot{\gamma} t_0 = 7$; it diverges at $\dot{\gamma}(t - t_0) = 4$ owing to compression ($T_{min} < 0$).

simple shear flow. For $\varepsilon > \varepsilon_H$ the capsule deformation increases with time without bound and the numerical computation has to be stopped. Changing the initial position of the poles, starting from the initial spherical shape or from a converged stable equilibrium shape, all lead to the same conclusion. To illustrate the point, we start from the stable equilibrium state (see figure 3) obtained for $\varepsilon = 0.6$ and a fine 40×80 mesh, and we increase ε to 1.2. The deformation D_{12} increases with time (figure 7*a*) up to a value of about 0.65 and then diverges. The shapes obtained in this fashion are very deformed owing to the large value of the capillary number and exhibit protruded tips, as shown in figure 8(*a*) for $\varepsilon = 1.2$, a short time before the simulation

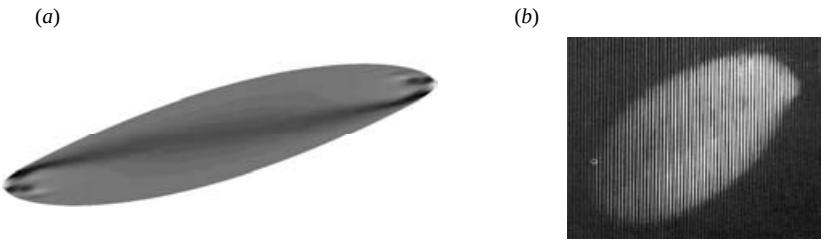

FIGURE 8. (*a*) Deformed capsule in simple shear flow for $\varepsilon = 1.2 > \varepsilon_H$, a few iterations before the calculation diverges (NH membrane); (*b*) photograph of a nylon membrane capsule just before burst (Chang & Olbricht 1993*b*).

breaks down. Such tips have also been observed experimentally by Chang & Olbricht (1993*b*) right before the capsule breaks up (figure 8*b*), albeit for small values of the viscosity ratio. To understand what happens, we have plotted the time evolution of the minimum principal tension T_{min} in the membrane. As shown in figure 7(*b*), the initial value of T_{min} is small but positive, but as the deformation increases, T_{min} decreases to negative values until buckling occurs and the computation has to be stopped. In this case, the compression areas are not located near the equator of the deformed shape, as observed for small shear rates, but appear near the tips. Consequently, buckling occurs in the protruded areas and leads to an instability of the numerical scheme. Compression is due to the torque exerted by the flow vorticity on the global deformed profile of the capsule. Indeed, the torque applied to a slender deformed capsule leads to flexural like deformation where parts of it undergo compression.

An issue can be raised regarding the ability of the numerical method to capture large deformations accurately. Indeed, the largest steady deformation D_{12}^{∞} obtained for an NH membrane capsule is about 56%, for $\varepsilon = 0.75$. In order to address this issue, computations were performed for a spherical capsule with a membrane obeying Navot's (1998) elastic law, (2.11). As was pointed out, such a membrane is never under compression. In particular, for $\varepsilon = 1.8$ (corresponding to $p = 6$ in Navot's simulations) a final deformation $D_{12}^{\infty} = 0.836$ is obtained with our method (figure 9), to be compared to Navot's result $D_{12}^{\infty} = 0.83$. Since the tensions are always positive, the capsule does not buckle and reaches a steady equilibrium state with a tank-treading motion. However, it was necessary to use 50×100 elements on the capsule surface to compute accurately the geometry of the deformed membrane, owing to high curvatures. This shows that the instability observed for an NH membrane when $\varepsilon > \varepsilon_H$ is of physical rather than numerical origin. Capsules with a membrane that obeys the SK law, also have protruding tips where compression occurs for values of ε larger than a critical value ε_H that increases with C, as shown in table 1.

At this point, it is important to consider certain issues in connection with the study by Ramanujan & Pozrikidis (1998). These authors mention numerical problems for capillary numbers larger than those for which a stable steady configuration was obtained in the present study. They point out the importance of bending resistance in avoiding them, but state that a critical shear rate does not exist and that the capsule always exhibits a steady deformation. It should also be noted that when we use the constitutive law (2.9) of Ramanujan & Pozrikidis (1998) we again find an upper threshold ε_H for obtaining equilibrium shapes, which is slightly larger than that found for NH membranes.

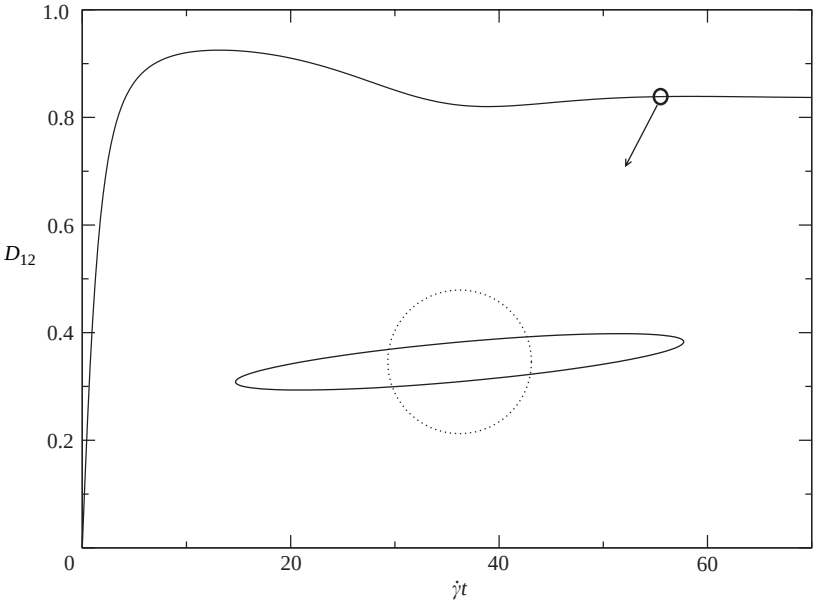

FIGURE 9. Deformation *vs.* time of a capsule in simple shear flow, for a membrane obeying law (2.11) with $\varepsilon = 1.8$. Insert: initial and steady deformed profiles in the shear plane at time $\dot{\gamma}t = 55$.

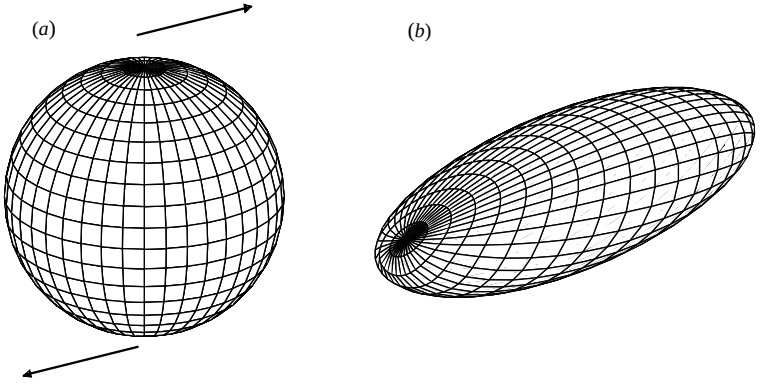

FIGURE 10. Three-dimensional representation of a capsule in simple shear flow ($\varepsilon = 0.6$, NH membrane); (*a*) at $t = 0$, (*b*) at stable steady state.

4.3. *Moderate shear rates* ($\varepsilon_L < \varepsilon < \varepsilon_H$)

There exist values of capillary number for which stable equilibrium is reached. The dynamic behaviour of a capsule in such conditions is described in this subsection. As shown in figure 3, the computation can proceed for times $\dot{\gamma}t$ very long compared to the transient time between the start of the flow and the onset of the tank-treading motion. A three-dimensional representation (figure 10) of the capsule shows that the deformed shape is smooth without folds. Similarly, the equilibrium capsule profiles for $C = 1$ are shown in figure 11 for different values of ε. As ε increases, the capsule becomes more elongated in the plane of shear at steady state. The variation of D_{12}^{∞} as a function of ε is shown in figure 4(*a*) for different membrane laws. Owing to the

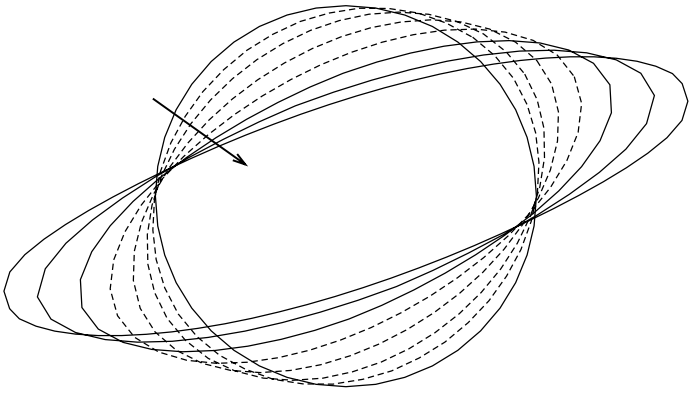

FIGURE 11. Steady deformed profiles of a capsule in simple shear flow (SK membrane, $C = 1$) for $\varepsilon = 0, 0.0375, 0.075, 0.15, 0.3, 0.6, 1.2$ and 2.1. The dashed lines show the unstable states and the arrow indicates increasing values of ε.

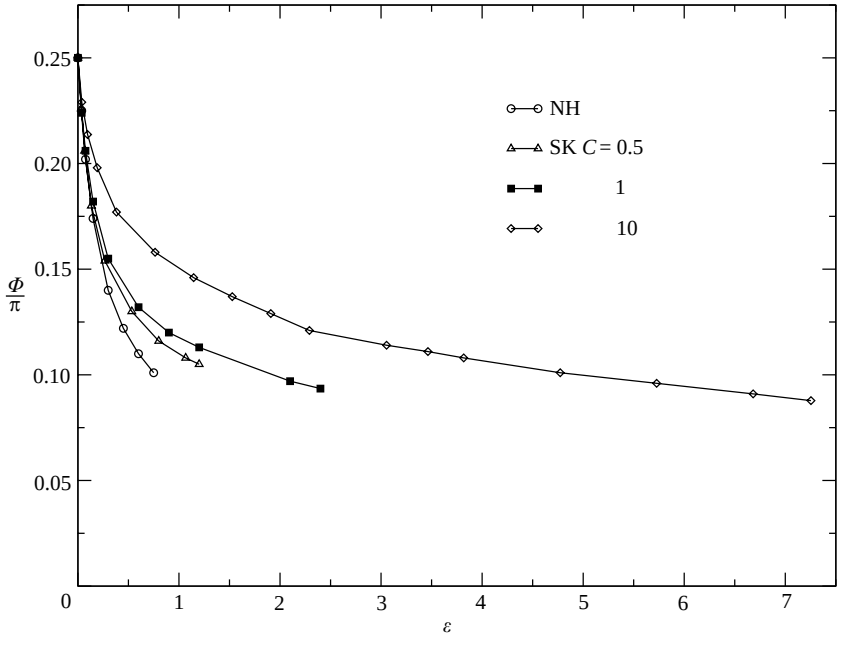

FIGURE 12. Inclination angle Φ with respect to the far flow field direction as a function of ε for a capsule in simple shear flow.

strain hardening behaviour of the SK law, a capsule with an SK membrane is less deformed than an NH capsule subjected to the same shear rate. This effect is more pronounced as C increases, i.e. as the membrane becomes more area incompressible. The inclination angle Φ with respect to the oncoming flow direction decreases owing to the increasing torque exerted upon the capsule (figure 12*a*). Note that the strain hardening effect delays the alignment of the capsule with streamlines.

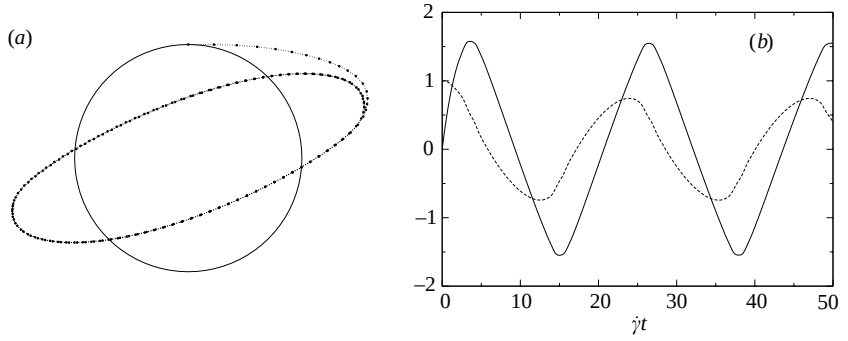

FIGURE 13. Capsule in simple shear flow; (*a*) trajectory of a membrane material point in the shear plane (x_1, x_2) ($\varepsilon = 0.6$, NH law); ○, the last position of the point at dimensionless time $\dot{\gamma}t = 50$, after two full circumvolutions in the shear plane; (*b*) coordinates x_1/a (continuous line) and x_2/a (dashed line) of the material point as functions of time.

For stable situations ($\varepsilon_L < \varepsilon < \varepsilon_H$), the motion of the capsule can be followed over long times, corresponding to two full circumvolutions in most cases. This behaviour is illustrated for an NH capsule by the trajectory of a membrane material point on figure 13(*a*). Two periods of tank treading motion are covered, as shown by the time variation of the coordinates of this point (figure 13*b*). It is then possible to determine the period $\dot{\gamma}T$ of the tank-treading motion from the time evolution of the position of a membrane material point in the shear plane. When equilibrium is reached, i.e. when the normal velocity of the membrane is less than $0.01\dot{\gamma}a$ everywhere, an instantaneous value of $\dot{\gamma}T$ can be obtained by integrating $\mathrm{d}l/|v|$ where $\mathrm{d}l$ is a line element over the capsule profile in the (x_1, x_2)-plane. For stable equilibrium, the values of $\dot{\gamma}T$ computed with the two methods are identical within numerical errors (of about 2%). The advantage of the second method is that it allows determination of a theoretical rotation period, even when we could not observe it because of the buckling instability discussed previously. The equilibrium rotation period is plotted as a function of ε and membrane rheology on figure 14(*a*). We find that $\dot{\gamma}T$ increases with ε and depends on the membrane constitutive law (figure 14*a*). In particular, for the same ε, i.e. for the same $\dot{\gamma}$ and G_s, the rotation period decreases as C increases. This means that the angular velocities of the two capsules are different and depend on C. Measuring the period of the tank-treading motion as a function of ε may thus lead to the value of C. The angular velocity of a rigid sphere ($\varepsilon \to 0$) in a simple shear flow is $\omega_O = \dot{\gamma}/2$, which corresponds to $\dot{\gamma}T_0 = 4\pi$.

However, when $\dot{\gamma}T$ is plotted as a function of the steady deformation D_{12}^{∞}, all points almost fall on the same curve (figure 14*b*). This suggests that the mean angular velocity of the membrane only depends on the capsule deformation, which depends in a nonlinear way on ε and membrane rheology (see figure 4). However, more results would be necessary to confirm this trend.

In conclusion, there is only a window of values for ε for which stable equilibrium shapes are obtained. Outside this range of values, buckling takes place and equilibrium shapes either exist but are unstable ($\varepsilon < \varepsilon_L$) or do not exist ($\varepsilon > \varepsilon_H$). To emphasize this point, we have plotted in figure 15*a*, *b*) the minimum T_{min} and maximum T_{max} values of the equilibrium principal tensions in the membrane as a function of ε for the four membrane laws. For small values of ε, T_{min} takes negative values (as predicted

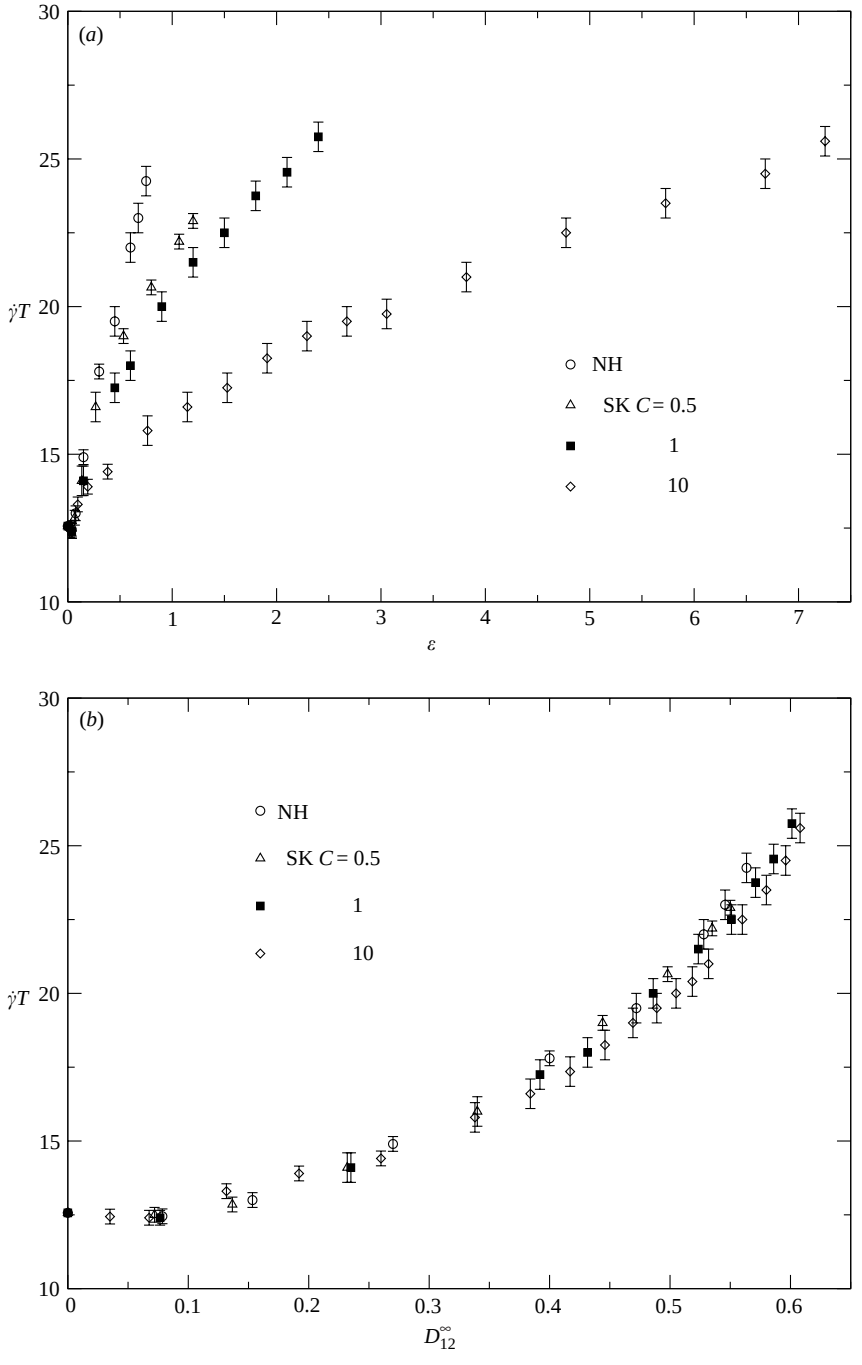

FIGURE 14. Tank-treading period as a function (*a*) of ε and (*b*) of D_{12}^{∞} for different membrane laws; for $\varepsilon = 0$, $\dot{\gamma}T = 4\pi$, corresponding to the rotation period of a rigid sphere in simple shear flow.

by the asymptotic analysis), the membrane is compressed and the equilibrium shapes are unstable. The limiting value ε_L reported in table 1, is inferred from this plot and corresponds to the point where T_{min} becomes positive. The process that increases T_{min}

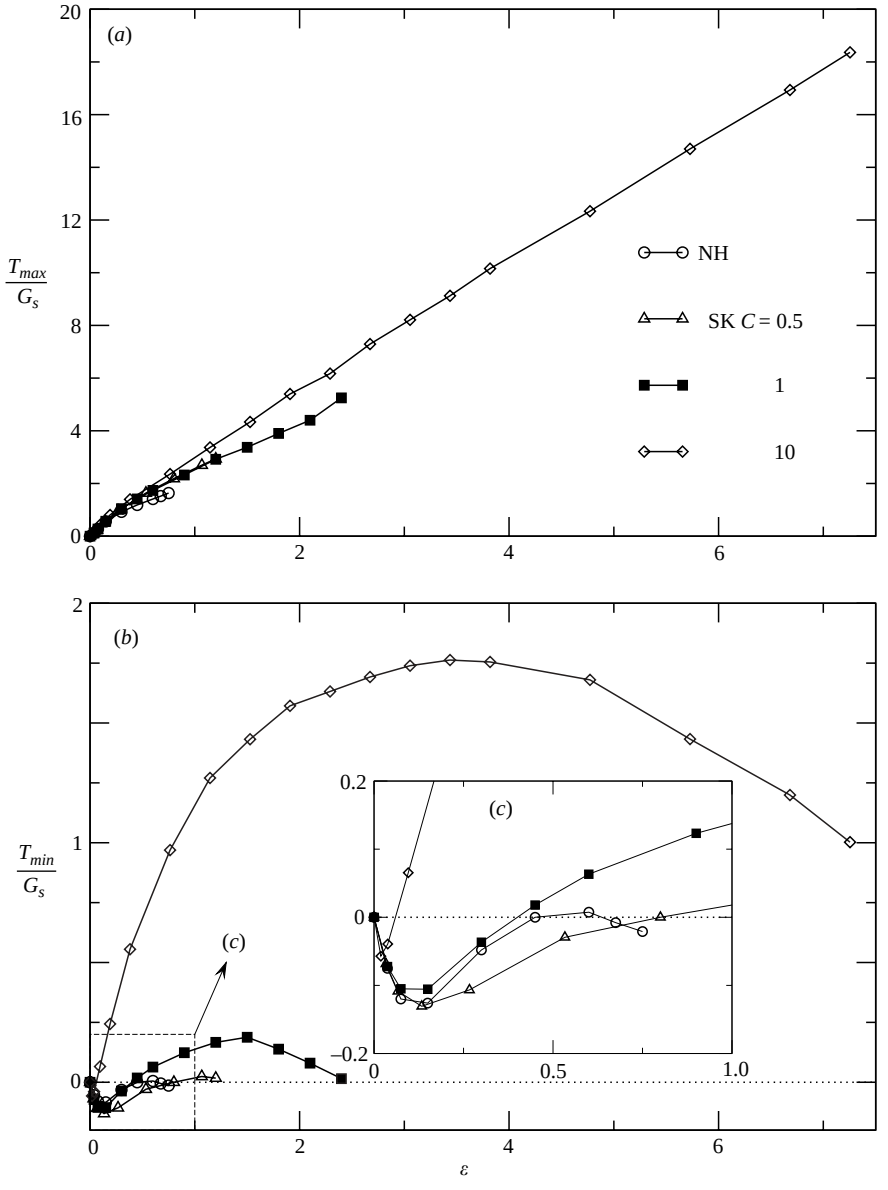

FIGURE 15. (*a*) Maximum and (*b*) minimum value of the principal tension in the membrane *vs.* ε for a spherical capsule in simple shear flow.

is linked to the area dilation of the membrane. Indeed, for $\varepsilon \ll 1$ the area dilation of the membrane is $O(\varepsilon^2)$. As ε increases, area dilatation is no longer negligible and its contribution to the tensions is weighted by K. Correspondingly, the values of ε_L decrease as C (or K/G_s) increases for an SK membrane, while the two values of ε_L are very close for NH and SK ($C = 1$) membranes that have the same area compression modulus.

As ε becomes large, T_{max} increases without bound, but T_{min} first increases and starts decreasing until it becomes negative. The second zero of T_{min} gives approximately

the value of ε_H, as reported in table 1. T_{min} becomes negative for high deformation because of the torsion of the overall deformed capsule caused by the viscous torque. This effect is apparent in figure 8, where the tips of the capsule are bent out of alignment.

At this point, we can now explain the effect of the initial position of the poles. When the computation begins, the capsule is undergoing small deformation and the membrane is under some compression for a short transient time, whatever the value of ε. In simple shear flow, the nodes are convected along the membrane. If the convection time is smaller than the advection time owing to compressive tension, the numerical representation of the membrane can sustain some compression. The worst situation occurs at the pole where the mesh size is smallest. Consequently, if the poles are located on the x_3-axis, they are quasi-stationary and subjected to compressive tensions. Since there is nothing to prevent overlapping of the nodes near the poles, the model breaks down quickly, even before any equilibrium can be reached. Depending on whether the poles are located on the x_1- or x_2-axis, they are convected towards or away from the compression area. For $\varepsilon < \varepsilon_L$, equilibrium can be reached, but the instability sets in sooner in the first case. For $\varepsilon > \varepsilon_L$, the tensions quickly become all positive and the pole position does not affect the equilibrium state of the capsule, as shown in figure 3.

5. Capsules in planar hyperbolic flow

A planar hyperbolic flow is devoid of vorticity, and, as such, is simpler than the shear flow studied previously. It can be generated experimentally in a four-roller flow cell (Bentley & Leal 1986), where the velocity field in Cartesian coordinates is given by

$$v_1^\infty(\boldsymbol{x}) = \dot{\gamma} x_1, \quad v_2^\infty(\boldsymbol{x}) = -\dot{\gamma} x_2, \quad v_3^\infty(\boldsymbol{x}) = 0. \tag{5.1}$$

For symmetry reasons, a capsule centred in the flow (5.1) reaches an equilibrium state (if any) where the membrane and the internal liquid are both motionless. The viscosity ratio has thus no influence on the equilibrium state. The major axes of the deformed profile are then aligned with the far flow directions x_1, x_2, x_3 with corresponding semi diameters L_1^∞, L_2^∞, L_3^∞. The Taylor deformation parameter D_{ij} is thus easily determined in each plane. To our knowledge, the large deformations of a capsule have not been modelled in this flow.

For $\varepsilon \ll 1$, the asymptotic theory of Barthès-Biesel *et al.* (2002) predicts the following values for flow (5.1)

$$\left.\begin{aligned} &\frac{L_1^\infty}{a} = 1 + \frac{5}{2}\frac{2+\nu_s}{1+\nu_s}\varepsilon, \quad \frac{L_2^\infty}{a} = 1 - \frac{5}{2}\frac{2+\nu_s}{1+\nu_s}\varepsilon, \quad \frac{L_3^\infty}{a} = 1 \\ &D_{12}^\infty = \frac{5}{2}\frac{2+\nu_s}{1+\nu_s}\varepsilon, \quad D_{23}^\infty = D_{13}^\infty = \frac{1}{2}D_{12}^\infty. \end{aligned}\right\} \tag{5.2}$$

The load on the membrane is given by (4.2), where the rate of strain now corresponds to flow (5.1). The solution of the membrane equilibrium equations in the spherical coordinate system defined in § 4.1, leads to the following asymptotic values of the tensions in the membrane

$$\frac{T^{\theta\theta}}{G_s} = 5\varepsilon\cos 2\phi, \quad \frac{T^{\phi\theta}}{G_s} = -5\varepsilon\cos\theta\sin 2\phi, \quad \frac{T^{\phi\phi}}{G_s} = -5\varepsilon\cos^2\theta\cos 2\phi. \tag{5.3}$$

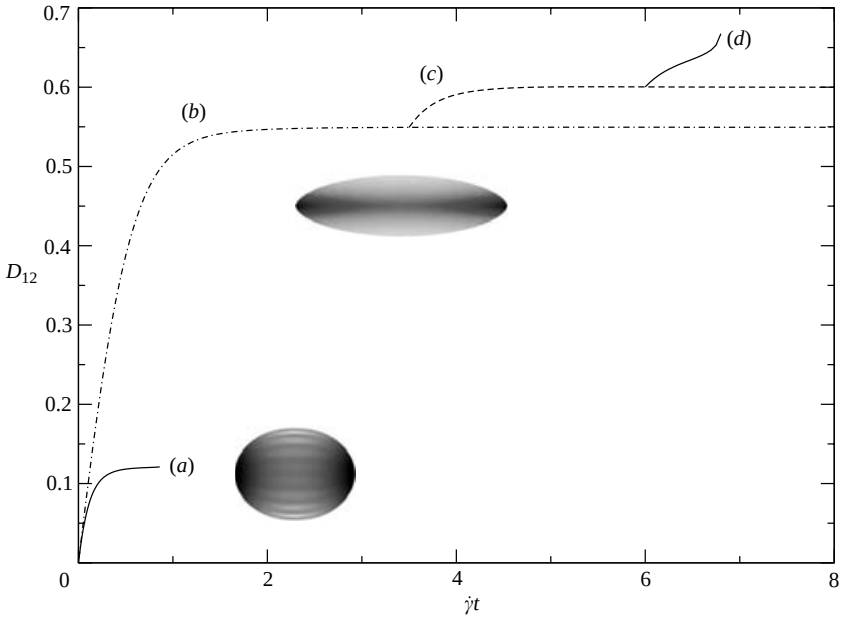

FIGURE 16. Capsule in hyperbolic flow (SK membrane – $C = 1$); time evolution of D_{12} for (*a*) $\varepsilon = 0.03 < \varepsilon_L$, (*b*) $\varepsilon = 0.45$, (*c*) $\varepsilon = 0.6$ and (*d*) $\varepsilon = 0.75 > \varepsilon_H$. Inserts: deformed capsule for $\varepsilon = 0.03$ at $\dot{\gamma}t = 0.87$ and for $\varepsilon = 0.45$ at $\dot{\gamma}t = 5$.

As compared to (4.3), the ϕ-dependency of the tension is different in hyperbolic flow because of the different orientation of the capsule with respect to the external flow. Negative tensions are thus also found in the membrane. For example, for membrane points in the extension plane x_1, x_2 ($\theta = \pi/2$), the only non-zero principal tension $T_\theta / G_s = 5\varepsilon \cos 2\phi$ acts in a direction perpendicular to the extension plane and is compressive in the middle of the capsule corresponding to

$$\phi \in \left[\frac{\pi}{4}, \frac{3\pi}{4}\right] \cup \left[\frac{5\pi}{4}, \frac{7\pi}{4}\right].$$

To illustrate the different phenomena, we discuss the case of a capsule with an SK ($C = 1$) membrane. Figure 16 shows the time evolution of the deformation D_{12} in the extension plane x_1, x_2 for typical values of ε. As for simple shear flow, the capsule reaches equilibrium after an initial transient phase. For small values of ε ($\varepsilon < \varepsilon_L$, here $\varepsilon_L = 0.15$), the equilibrium state is unstable because of compressive tensions. The membrane shows a tendency to buckle, as shown in figure 16(*a*). Again, since there is zero bending rigidity, the folds depend on the grid points position and do not model the actual buckling modes of the membrane, but indicate the location of the compression zones. A detailed study of the tension distribution in the membrane shows that there exist negative principal tensions located in the vicinity of the deformed capsule equator. For small values of ε, the asymptotic and numerical values of the tensions are in agreement. As ε increases, the maximum T_{max} and minimum T_{min} values of the principal tensions increase. Eventually, T_{min} which was originally negative, changes sign and that determines the value ε_L. For $\varepsilon > \varepsilon_L$, the principal tensions are then positive everywhere in the membrane. This case is illustrated for $\varepsilon = 0.45$ in figure 16(*b*), where the capsule reaches an equilibrium that is stable over long times. The membrane maximum velocity $|v_{max}/a\dot{\gamma}|$ is of the order of 10^{-5} at

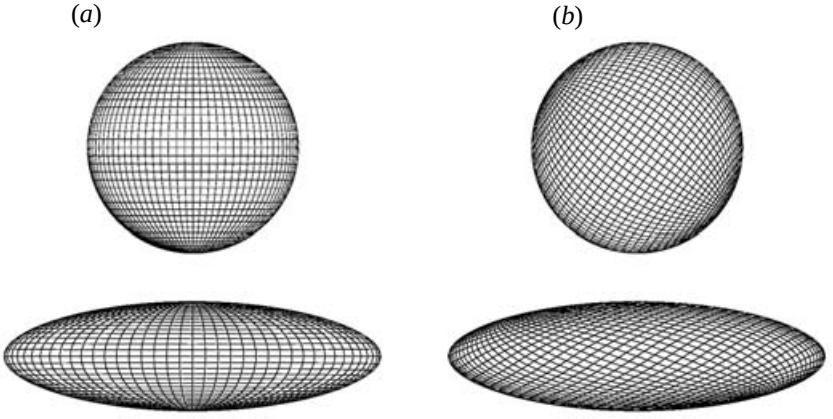

FIGURE 17. Capsule in hyperbolic flow. Identical stable equilibrium profiles (bottom) are reached for two different initial positions of the grid poles (top); SK law – $C=1$, $\varepsilon=0.45$, $\dot{\gamma}t=5$, $D_{12}^{\infty}=0.55$.

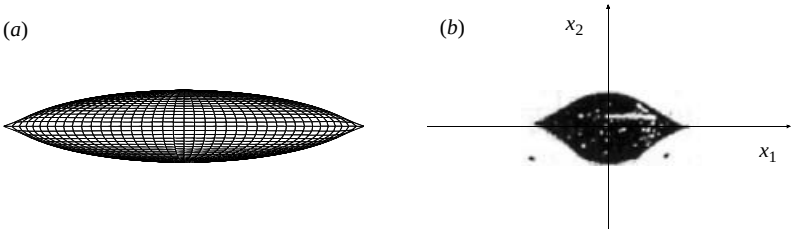

FIGURE 18. (*a*) (x_1, x_2) profile of a capsule in hyperbolic flow for $\varepsilon=0.75 > \varepsilon_H$ (SK $C=1$ law) before the simulation diverges; (*b*) photograph of a polylysine membrane capsule at burst (Barthès-Biesel 1991).

$\dot{\gamma}t=8$. The corresponding capsule profile is smooth (figure 16*b*). Changing the initial position of the poles changes neither the deformed profile nor its stability (figure 17). Again, the position of the poles has no influence, provided they are not located in the compression zone. If not, since the nodes move only during the transient phase, the instability sets in quickly and it is not possible to reach the equilibrium state. Starting from this equilibrium state, we increase ε to $\varepsilon=0.6$ (figure 16*c*). After a transient phase, the capsule reaches another steady equilibrium shape, which is identical to the one we would obtain starting from the initial spherical shape. When we increase ε past a limiting value ε_H (here $0.6<\varepsilon_H<0.75$), we cannot find any equilibrium state (figure 16*d*). Figure 18(*a*) shows what happens for $\varepsilon=0.75$: the capsule develops high-curvature protruded ends, and the deformation and the tensions in the membrane increase without bound. We thus observe a process of continuous extension, well-documented for liquid droplets. Barthès-Biesel (1991) also reports protruded shapes (figure 18*b*) for polylysine membrane capsules just before burst. The same features are observed for SK ($C=0.5, 1, 10$) membranes as well as NH membranes. The values of the two limits ε_L and ε_H depend on membrane properties and on flow type, as shown in table 1. As for simple shear flow and for the same reasons, the limit ε_L decreases as K/G_s increases.

The value ε_H is approximate and lies within an interval between the last stable and first unstable situation that we obtained. No attempt was made to determine ε_H with

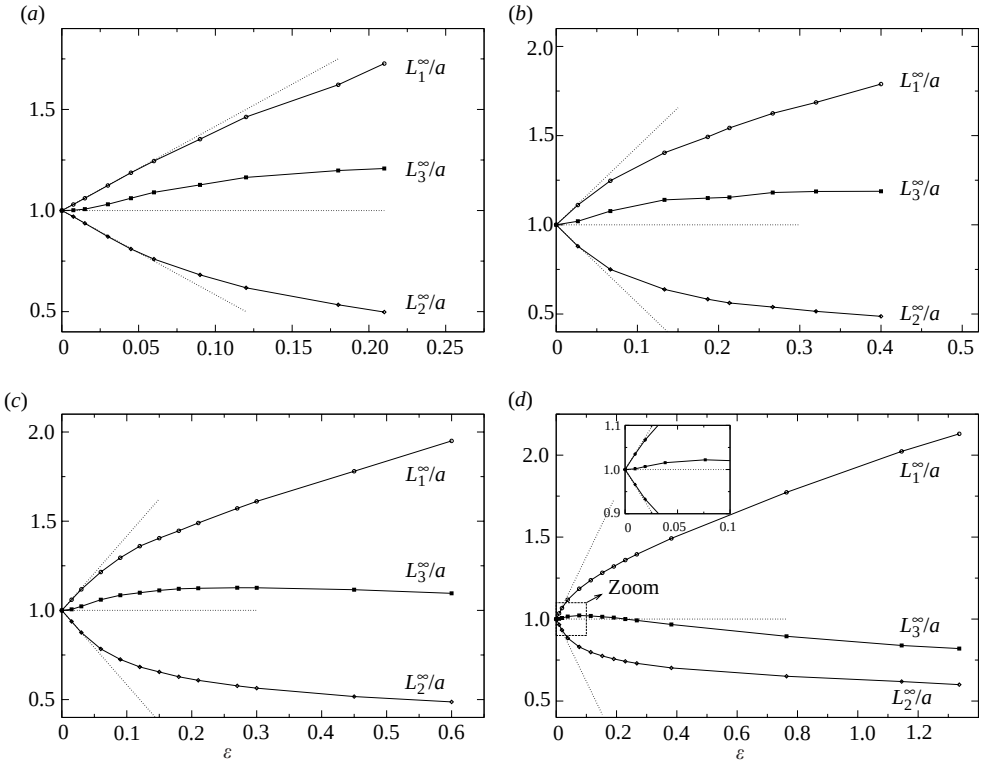

FIGURE 19. Capsule in plane hyperbolic flow. Semi axis lengths L_1^∞, L_2^∞, L_3^∞ as functions of ε for different membrane laws: (*a*) NH; (*b*) SK ($C = 0.5$); (*c*) SK ($C = 1$); (*d*) SK ($C = 10$). Dotted lines show asymptotic predictions.

greater precision. The value of deformation $(D_{12}^\infty)_H$ corresponds to the last stable deformation. It should be noted that the interval $[\varepsilon_L, \varepsilon_H]$ is small for capsules with an NH membrane.

It is of interest to discuss the equilibrium state of the capsule as a function of membrane properties. In the case of an SK ($C = 1$) membrane, the equilibrium values of the capsule semi diameters L_1^∞, L_2^∞, L_3^∞ (obtained before the instability sets in when $\varepsilon < \varepsilon_L$) are shown as a function of ε in figure 19(*c*). The asymptotic results are recovered within a few per cent up to $\varepsilon = 0.03$–0.04 for L_1^∞ and L_2^∞, but not for L_3^∞, for which the asymptotic theory predicts the constant value a. The deformation of the capsule is three-dimensional. As expected, in the (x_1, x_2)-plane, the profile is elongated along x_1 and flattened along x_2. However, in the transverse (x_2, x_3)-plane, the profile is more elongated along x_3 than along x_2, which was not obvious *a priori*. This feature is also observed for SK ($C = 0.5, 10$) and for NH membranes, although the stable equilibrium range is small in the latter case. The equilibrium values of L_1^∞, L_2^∞, L_3^∞, are shown as functions of ε in figures 19(a, b, d) for the NH and SK ($C = 0.5$ and 10) laws. From these values, it is easy to compute the values of the Taylor deformation in each plane.

For values of ε outside the range of validity of the asymptotic theory, large deformations (over 50%) are observed in the (x_1, x_2)-plane where D_{12} seems to increase continuously. The strain-hardening effect of the SK law leads to larger values of ε (i.e. larger values of the shear rate $\dot{\gamma}$) for $C = 10$ than for $C = 1$ to obtain the

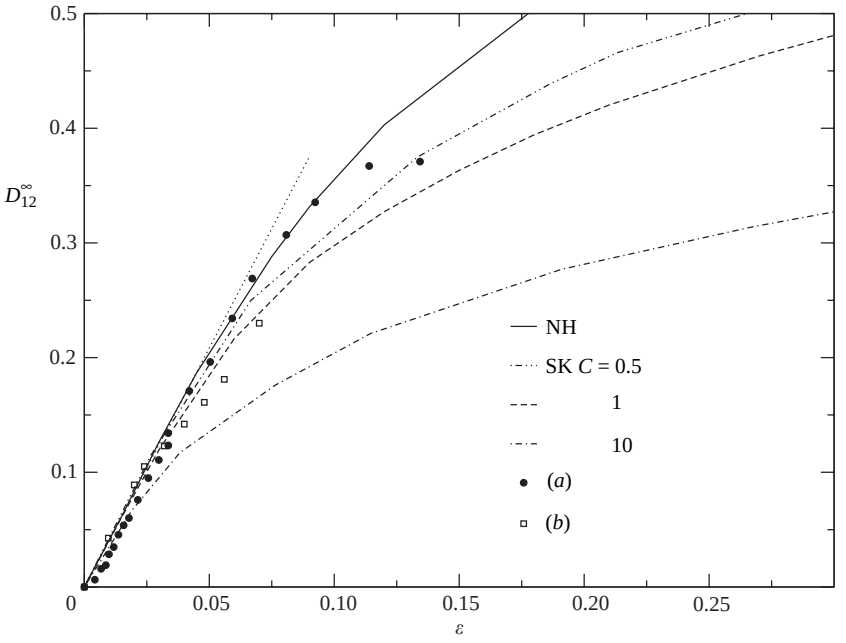

FIGURE 20. Spherical capsule in plane hyperbolic flow. Deformation as a function of ε for different membrane laws. Experimental data by (a) Chang & Olbricht (1993a) and (b) Barthès-Biesel (1991). The dotted line represents the asymptotic prediction used to rescale the experimental ε.

same deformation. In the transverse plane x_2, x_3, the two semi-diameters L_2^{∞} and L_3^{∞}, and thus the deformation D_{23}^{∞}, tend to level off as ε increases. This effect is observed for lower values of ε as C increases. Another view of the effect of membrane constitutive law is shown in figure 20 where D_{12}^{∞} is plotted as a function of ε for all four membrane laws. There are two experimental studies of the deformation of capsules in such a flow, with nylon (Chang & Olbricht 1993a) or polylysine membranes (Barthès-Biesel 1991). Since the viscosity ratio λ has no influence on the steady deformations D_{ij}^{∞}, we can compare our numerical results to experimental data, even if we have assumed $\lambda = 1$. The results of Barthès-Biesel (1991) and of Chang & Olbricht (1993a) are thus also shown in figure 20. A difficulty lies in the proper determination of G_s, and thus of ε. Indeed, Chang & Olbricht (1993a) evaluated the value of G_s either from compression experiments on a capsule, or from the initial slope of the deformation versus shear rate curve (as was done in figure 20). The two values could differ by 30%. For polylysine membrane capsules, the value of G_s is determined only from the initial slope of the deformation curve. Barthès-Biesel (1991) reports the appearance of protruded ends for a capsule with a polylysine membrane (figure 18b) where the membrane is punctured and some of the internal liquid is expelled. However, such lemon-shaped profiles are observed experimentally for values of ε much smaller than ε_H for NH or SK membranes. Chang & Olbricht (1993a) do not report any breakup for capsules with a nylon membrane in hyperbolic flow, but observe substantial permanent plastic deformation during the elongation process. This may be the reason why the final deformation seems to reach a plateau. A plastic behaviour of the membrane material is not accounted for in our model, and this may explain why the fit between numerical predictions and experiments is not better. For

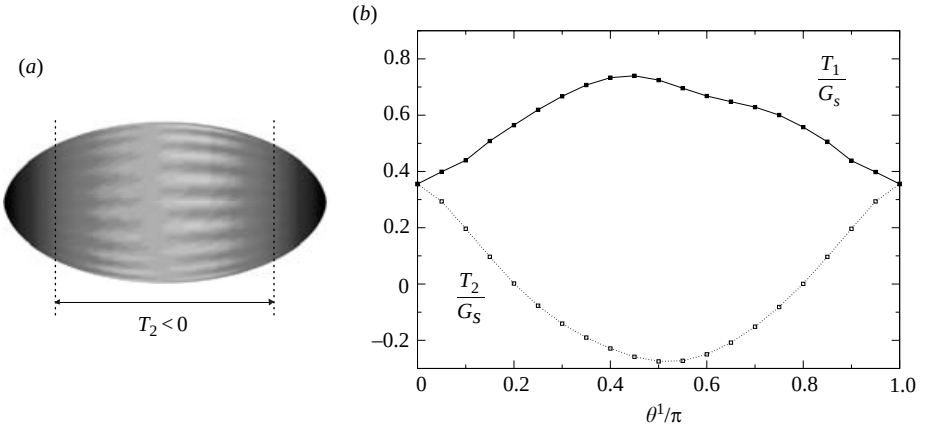

FIGURE 21. (*a*) Side view of a capsule deformed in axisymmetric elongational flow a few iterations before the calculation diverges ($\varepsilon = 0.09 < \varepsilon_L$, NH membrane). (*b*) Principal tensions in (x_1, x_2)-plane; left-right symmetry is broken in the region where $T_2 < 0$, i.e. for $0.2 < \theta^1/\pi < 0.8$.

low shear rate, membrane folding is not reported for any type of capsule. This may be linked to poor optical resolution of the observation system, or to the flexural rigidity of the membrane owing to a finite thickness. It is clear that more experimental results are required for this type of flow.

6. Capsules in axisymmetric elongational flow

An axisymmetric elongational flow is given in Cartesian coordinates by

$$v_1^\infty(\boldsymbol{x}) = 2\dot{\gamma} x_1, \quad v_2^\infty(\boldsymbol{x}) = -\dot{\gamma} x_2, \quad v_3^\infty(\boldsymbol{x}) = -\dot{\gamma} x_3. \tag{6.1}$$

Barthès-Biesel *et al.* (2002) studied the deformation of an initially spherical capsule suspended in a flow field described by (6.1). They took advantage of the problem axisymmetry to first integrate (2.1) in the azimuthal direction and to reduce it to a line integral along a meridian curve of the capsule interface. The capsule profile was thus *a priori* assumed to be axisymmetric and the principal directions of deformation and tension were along the meridian and parallel lines. No buckling instability was detected because the meridian lines were always stretched, and equilibrium solutions were obtained for values of ε lower than an upper limit. Here, we remove the axisymmetry constraint and treat the problem as three-dimensional.

Stable situations were encountered only for capsules with an SK ($C = 10$) membrane. In this case, the three-dimensional simulations are in very good agreement with the axisymmetric model. There is less than 1% difference on the value of D_{12}^∞ in the range of capillary numbers where a stable steady state was obtained. We estimate this window of stability to lie between $\varepsilon_L = 0.02$ and $\varepsilon_H = 0.76$. For the NH law or the SK ($C = 1$) law, corresponding to more deformable membranes, the axisymmetry of the flow always generates negative tensions and we could not find a value for ε_L. The typical response of the capsule is illustrated for an NH membrane with $\varepsilon = 0.09$. Figure 21(*b*) shows the values of the principal tensions in the (x_1, x_2)-plane, as a function of θ^1 measured along the meridian. We find negative values of tension T_2 along parallel lines in the vicinity of the capsule equator. The capsule membrane thus tends to buckle in this area as shown in figure 21(*a*) and the computation must

be terminated. In the axisymmetric model of Barthès-Biesel *et al.* (2002), negative hoop tensions were also obtained, but their influence on the three-dimensional stability of the problem was ignored.

Similar situations occur when a capsule is flowing into a cylindrical tube where axisymmetry is also assumed. Compressive tensions may then appear in the azimuthal direction, as well as in some parts of the meridians, particularly at the back of the capsule. Diaz & Barthès-Biesel (2002) then found it necessary to add some bending resistance to the membrane in order to stabilize the shape of the capsule. When the bending modulus is small enough, the front part of the capsule profile, the liquid film thickness around it and the additionnal pressure drop are only slightly modified. This indicates that a small amount of bending resistance can be enough to sustain the compressive tensions that arise in the membrane without affecting substantially the shape of the capsule deformed profile. Obviously, as the bending rigidity is increased the shape of the capsule will be changed, as shown by Kwak & Pozrikidis (2001) or by Pozrikidis (2001).

7. Discussion

Based on three different flow situations and two commonly used membrane constitutive laws, we have shown that a simple membrane behaviour where bending resistance is neglected limits the numerical simulations to situations where the model is physically correct. This is a recurring theme of this study that persists when membranes described by different laws are considered under various three-dimensional Stokes flow patterns.

It is of interest to compare the behaviour of the capsule in simple shear and plane hyperbolic flow. As the shear rate is measured differently in the two flows, we use the equilibrium deformation in the shear plane as a comparison parameter. The maximum and minimum values of principal tensions in the membrane are then plotted as a function of D_{12}^{∞} for NH and SK ($C = 0.5$, 1, 10) laws in figure 22. We then find almost identical dependence of T_{max} and T_{min} upon D_{12}^{∞} for simple shear and plane hyperbolic flow. This is because the capsule is stretched in a similar fashion in both flows: along the x_1-axis in the hyperbolic case and along a direction making the angle Φ with the streamlines in the simple shear case (see figure 12). The maximum principal tension T_{max} is positive and increases without any clear bound as D_{12}^{∞} and thus ε increases. The minimum principal tension behaves differently: T_{min} first decreases to negative values for small deformation (as predicted by the asymptotic analysis) and then, as D_{12}^{∞} increases, T_{min} increases and becomes positive. The D_{12}^{∞} value for which T_{min} is zero corresponds to $\varepsilon = \varepsilon_L$. For both flows, the change of sign of T_{min} occurs for very close values $(D_{12}^{\infty})_L$ of deformation for a given membrane constitutive law (table 1). The corresponding values of ε_L are different because the shear rate is not evaluated in the same way. Except for the SK ($C = 10$) law, there is no simple correspondence (such as a 1/2 factor, as might be expected from the asymptotic tension values) between the values of ε_L in simple shear and plane hyperbolic flows. This is probably because ε_L corresponds to high enough values of the capillary number where the simple linear asymptotic theory no longer applies and where the deformation mechanics are already nonlinear. However, for an SK membrane with $C = 10$, the value of $(D_{12}^{\infty})_L$ is small enough for the asymptotic analysis to apply, and we indeed find that ε_L for simple shear is half of ε_L for hyperbolic flow.

As ε and D_{12}^{∞} increase, T_{min} increases without any apparent bound for hyperbolic flow, but suddenly starts decreasing and tends to become negative again in simple

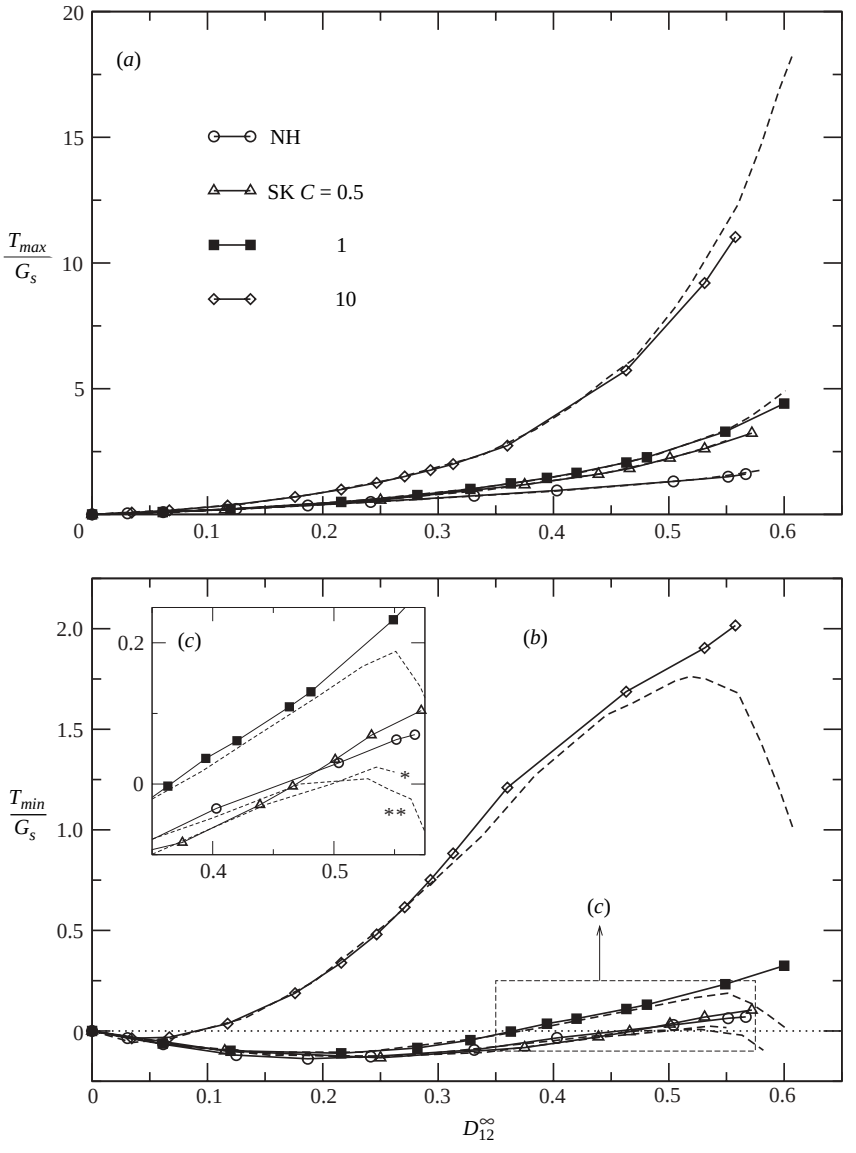

FIGURE 22. (*a*) Maximum and (*b*) minimum value of the principal tension in the membrane *vs.* D_{12}^{∞}; comparison between the simple shear flow (dashed lines) and the planar hyperbolic flow (solid lines). In insert, * points to SK ($C = 0.5$) law; ** points to NH law.

shear flow (figure 22). For large values of D_{12}^{∞}, the capsule is very elongated and has a large curvature at the tips. The difference between the two flows is attributed to the torque that is present in simple shear and absent in hyperbolic flow. The exerted torque tends to bend the whole capsule, thus leading to a distortion of the overall shape where the tips are out of alignment (figure 9) and where negative tensions appear in the bent parts of the capsule near the tips. The value $(D_{12}^{\infty})_H$ for which T_{min} becomes negative again determines the value ε_H for simple shear flow. In the case of hyperbolic flow, such a simple criterion cannot be found, ε_H must be determined by trial and error and $(D_{12}^{\infty})_H$ corresponds to the last stable deformation we computed.

The comparison between the two flows then leads to the conclusion that the large ε behaviour is essentially identical in both cases: the capsule undergoes continuous extension past a critical value ε_H of shear rate. However, for simple shear flow, the combination of very protruded shapes and viscous torque leads to compressed zones in the capsule interface where the simplified membrane model breaks down and buckling occurs. In both flows, we find roughly the same critical value $(D_{12}^{\infty})_H$. This unique dependency on D_{12}^{∞} is surprising since the Taylor deformation parameter is a global deformation measure that is insensitive to homothetic scaling. Furthermore, capsule response to hydrodynamic stresses is a three-dimensional nonlinear process that involves two flow fields (internal and external) for simple shear and only the external flow for plane hyperbolic flow.

We can also use these results to assess the effect of membrane constitutive law on the capsule dynamics. For SK law with different values of C, we find that $(D_{12}^{\infty})_L$ and ε_L decrease as C and surface Poisson ratio ν_s increase (see table 1), i.e. as the area dilation modulus K increases. We can also compare NH and SK ($C=1$) laws, that have the same small-deformation behaviour, but different large-deformation effects. We find that the values of ε_L and $(D_{12}^{\infty})_L$ are close for both the simple shear and the planar hyperbolic flow, indicating that ε_L could be a function of the elastic constants G_s and K (and/or G_s and ν_s).

The maximum stable deformation is of the same order for all membrane laws and for the two flows. However, the corresponding upper limit ε_H increases as C increases, and depends on the type of flow. This may be because ε measures the ratio of viscous to shear elastic stresses and accounts for neither the area dilation modulus nor for nonlinear large-deformation behaviour (such as strain hardening). This appears clearly when comparing the values of ε_H for NH and SK ($C=1$) membranes. Although the two laws have the same small-deformation values of G_s and K, they lead to different large-deformation behaviours where NH law is strain softening whereas SK law is strain hardening. It follows that the value of ε_H for the SK ($C=1$) membrane is about three times larger than the value of ε_H for the NH membrane.

We showed that compressive tensions on the membrane rendered the well-known equilibrium shapes unstable, giving rise to what looked like a wrinkled shape. The asymptotic theory predicts the appearance of negative tensions in any external flow situation for small enough capillary numbers, but is unable to give the maximum value ε_L until this occurs. Only the numerical model can do so. Since the membrane has no flexural rigidity, it buckles as soon as the tensions become compressive. The source of errors, and consequently of the deviation from the equilibrium shape, is located at the nodes of the surface and this explains why the wrinkle wavelength is locally dependent on the mesh size. It would thus be interesting to add some bending resistance to the membrane in order to model the buckling of the interface. As shown by shell and plate stability theory (Timoshenko & Gere 1961), the wavelength of a buckling instability tends to zero as the bending modulus vanishes. However, predicting numerically the first instability mode in small deformations with a proper shell model will presumably be very costly for numerical stability reasons. Indeed, to be able to capture a buckling mode of wavelength $2h$, we require a mesh with characteristic size smaller than h. In terms of numerical stability, we saw that the time step Δt had to be decreased as h decreases. Consequently, a small bending modulus implies a small wrinkle wavelength, which finally requires a fine mesh and a small time step to capture the instability. On the other hand, if we try to shorten the computation by reducing the number of elements in the mesh, we require a larger

bending modulus to capture a larger wavelength. However, according to Pozrikidis (2001) the value of the bending modulus further reduces Δt owing to the additional rigidity of the structure. We can thus expect that the time step will always have to be extremely small, especially in the domain of small deformations since a small value of ε is another factor that reduces Δt. Wrinkles have been observed experimentally for some capsules undergoing small deformations (Walter *et al.* 2001). In the experiments, the wrinkled shape of the capsule is stable, because the membrane has a small finite-bending resistance corresponding to a non-zero thickness. The measurement of the wrinkle wavelength coupled to a proper model of capsule deformation including bending rigidity may then be a good way to determine the bending modulus of such thin membranes. Note that the capsule buckling that arises for $\varepsilon < \varepsilon_L$ (i.e. when shear is small, compared to elasticity) resembles the elastically driven instabilities regularly observed in viscoelastic flows at high Deborah numbers (i.e. high elasticity compared to shear). For example, in annular extrusion flows, a standing wave is caused by gravity pulling the extruded annular film downward, a phenomenon that Schaul, Hannon & Wissbrun (1975) called pleating or curtaining because of the film shape. The grooves wavelength and amplitude depend on the extrusion conditions and fluid properties (Giesekus 1972; Piau, El Kissi & Tremblay 1990). Here, instead of gravity pulling down a film, we have weak shear forces stretching a capsule membrane.

For large shear rates ($\varepsilon > \varepsilon_H$), equilibrium shapes could not be obtained, irrespective of the membrane constitutive law and the position of the poles. This phenomenon is not due to numerical errors in the evaluation of the membrane deformation, since stable steady elongated shapes, with high curvature and a deformation D_{12}^{∞} larger than 80% could be obtained for the membrane constitutive law proposed by Navot (1998), that precludes the development of compressive stresses. As shown by Pozrikidis (2001), adding bending resistance changes the shape of the capsule for a given value of ε by decreasing the tip curvature, among other effects. However, if the shear rate is increased to high enough levels, it is not clear whether bending resistance can prevent the process of continuous elongation and global shape distortion altogether. It might be conjectured that the stability interval will be shifted to lower ε_L and higher ε_H when bending resistance is included. This point needs more investigation, but is in contradiction to Ramanujan & Pozrikidis (1998), who concluded that there is no critical shear rate beyond which steady deformation is not observed and attributed the findings of Pozrikidis (1995) to numerical error.

The authors wish to express their great appreciation for the bilateral French–Greek Research Program 'PLATO' that enabled this collaborative work. They are very grateful to Professor Heinz Rehage for his collaboration and fruitful discussions on the experimental work conducted at the University of Essen, Germany. Discussions with Dr Spyros Karamanos from the Department of Mechanical Engineering of the University of Thessaly on the subjects of shell dynamics and buckling were also appreciated.

REFERENCES

Barthès-Biesel, D. 1980 Motion of a spherical microcapsule freely suspended in a linear shear flow. *J. Fluid Mech.* **100**, 831–853.

Barthès-Biesel, D. 1991 Role of interfacial properties on the motion and deformation of capsules in shear flow. *Physica* A: *Statist. Theor. Phys.* **172**, 103–124.

Barthès-Biesel, D., Diaz, A. & Dhenin, E. 2002 Effect of constitutive law for two dimensional membranes on flow-induced capsule deformation. *J. Fluid Mech.* **460**, 211–222.

Barthès-Biesel, D. & Rallison, J. M. 1981 The time-dependent deformation of a capsule freely suspended in a linear shear flow. *J. Fluid Mech.* **113**, 251–267.

Bentley B. J. & Leal L. G. 1986 An experimental investigation of drop deformation and breakup in steady, two-dimensional linear flows. *J. Fluid Mech.* **167**, 241–283.

Chang, K. S. & Olbricht, W. L. 1993*a* Experimental studies of the deformation and break-up of a synthetic capsule in extensional flow. *J. Fluid Mech.* **250**, 587–608.

Chang, K. S. & Olbricht, W. L. 1993*b*. Experimental studies of the deformation and break-up of a synthetic capsule in steady and unsteady simple shear flow. *J. Fluid Mech.* **250**, 609–633.

Diaz, A., Pelekasis, N. & Barthès-Biesel, D. 2000 Transient response of a capsule subjected to varying flow conditions: effect of internal fluid viscosity and membrane elasticity. *Phys. Fluids* **12**, 948–957.

Diaz, A. & Barthès-Biesel, D. 2002 Entrance of a bioartificial capsule in a pore. *Comput. Model. Engng Sci.* **3** (3), 321–337.

Eggleton, C. D. & Popel, A. S. 1998 Large deformation of red blood cell ghosts in a simple shear flow. *Phys. Fluids* **10**, 1834–1845.

Giesekus, H. 1972 On instabilities in Poiseuille and Couette flows of viscoelastic fluids. *Progr. Heat Mass Transfer* **5**, 187–193.

Green, A. E. & Adkins, J. E. 1960 *Large Elastic Deformations.* Oxford University Press.

Kraus, M., Wintz, W., Seifert, U. & Lipowsky, R. 1996 Fluid vesicle in shear flow. *Phys. Rev. Lett.* **77**, 3685–3688.

Kwak, S. & Pozrikidis, C. 2001 Effect of membrane bending stiffness on the deformation of capsules in uniaxial extensional flow. *Phys. Fluids* **13**, 1234–1242.

Li, X. Z., Barthès-Biesel, D. & Helmy, A. 1988 Large deformations and burst of a capsule freely suspended in an elongational flow. *J. Fluid Mech.* **187**, 179–196.

Navot, Y. 1998 Elastic membranes in viscous shear flows. *Phys. Fluids* **10**, 1819–1833.

Pfafferott, C., Wenby, R. & Meiselman, H. J. 1985 Red blood cell deformation in shear flow. Effects of internal and external phase viscosity and of in vivo aging. *Biophys. J.* **47**, 695–704.

Piau J. M., El Kissi N. & Tremblay B. 1990 Influence of upstream instabilities and wall slip on melt fracture and sharkskin phenomena during silicones extrusion through orifices dies. *J. Non-Newtonian Fluid Mech.* **24**, 145–180.

Pozrikidis, C. 1990 The axisymmetric deformation of a red blood cell in uniaxial straining Stokes flow. *J. Fluid Mech.* **216**, 231–254.

Pozrikidis, C. 1992 *Boundary Integral and Singularity Methods for Linearized Viscous Flow* Cambridge University Press.

Pozrikidis, C. 1995 Finite deformation of liquid capsules enclosed by elastic membranes in simple shear flow. *J. Fluid Mech.* **297**, 123–152.

Pozrikidis, C. 2001 Effect of membrane bending stiffness on the deformation of capsules in simple shear flow. *J. Fluid Mech.* **440**, 269–291.

Prenter, P. M. 1989 *Splines and Variational Methods.* John Wiley and Sons.

Rallison, J. M. & Acrivos, A. 1978 A numerical study of the deformation and burst of a liquid viscous drop in extensional flow. *J. Fluid Mech.* **89**, 191–200.

Ramanujan, S. & Pozrikidis, C. 1998 Deformation of liquid capsules enclosed by elastic membranes in simple shear flow: large deformations and the effect of fluid viscosities. *J. Fluid Mech.* **361**, 117–143.

Schaul, J. S. Hannon, M. J. & Wissbrun, K. F. 1975 Analysis of the factors determining Parison properties in high shear rate blow molding. *Trans. Soc. Rheol.* **19**, 351–370.

Schmid-Schönbein, H. & Wells, R. E. 1960 Fluid drop like transition of erythrocytes under shear. *Science* **165**, 288–291.

Skalak, R., Tozeren, A., Zarda, R. P. & Chien, S. 1973 Strain energy function of red blood cell membranes. *Biophys. J.* **13**, 245–264.

Timoshenko, S. P. & Gere, J. M. 1961 *Theory of Elastic Stability*. McGraw-Hill.

Walter, A., Rehage, H. & Leonhard, H. 2000 Shear-induced deformation of polyamid microcapsules. *Colloid Polymer Sci.* **278**, 169–175.

Walter, A., Rehage, H. & Leonhard, H. 2001 Shear induced deformation of microcapsules: shape oscillations and membrane folding. *Colloids Surfaces* A: *Physicochem. Engng Aspects* **183–185**, 123–132.